*Journal of Structural Geology*, Vol. 5, No. 3/4, pp. 351 to 368, 1983
Printed in Great Britain

0191-8141/83 $3.00 + 0.00


# A theory of finite strain variation through contrasting layers, and its bearing on cleavage refraction

SUSAN H. TREAGUS

Department of Geology, The University, Manchester, M13 9PL, U.K.

(*Received* 23 *March* 1982; *accepted in revised form* 14 *December 1982*)

**Abstract**—A theory of finite strain variation in contrasting viscous layers is presented. The theory is applicable to layers which are oblique to two principal strains, but parallel to the third, and is not restricted to plane strain. Results may be obtained algebraically or by use of the Mohr diagram for strain. Solutions are given for various examples of layering attitude and viscosity ratio, measured with respect to a reference layer. It is shown that the finite strain ellipsoid changes in shape and orientation across contrasting layers, and in some cases the principal axes may be exchanged. Low strain is indicated in relatively more viscous layers, and high strain with extension at a smaller angle to the layering, in less viscous layers; the latter may approximate simple shear parallel to layering if the strain is sufficiently high.

The geological implications of the theory are strong strain variations in layered rock sequences. It is suggested that, in general, strain will be inhomogeneous from layer to layer both in orientation and amount. The relationship of strain and cleavage are reviewed in the Introduction to establish the validity of predicting cleavage patterns from strain data. Qualitative comparisons between the theoretical results of strain variation and natural cleavage refraction in layered rocks would appear to justify the assumption that cleavages of varied morphologies are sub parallel to the *XY* planes of strain. With this assumption, some three-dimensional features of planar and linear fabric refraction in contrasting rocks are predicted.

## INTRODUCTION

THE VARIATION of strain in different lithologies may be studied through measurements of strained objects, geometric studies of structures such as folds, and rock fabric studies. However, strain markers rarely occur in abundance throughout a sequence of rock types; they are more usually confined to a particular lithology. The geometry of folds can only be used for strain data if certain assumptions of fold mechanism are made. Probably the most commonly observed structures in deformed rocks are the rock fabric structures, foliations such as cleavage and schistosity and 'stretching' or mineral elongations. In deformed sedimentary and low-grade metamorphic rocks the rock fabric is generally identified in the field by macroscopic first cleavage planes at measurable angles to bedding planes, in both folded and unfolded rocks. The morphological nature of cleavage in particular lithologies and its variation in orientation may provide valuable strain data in rocks without strain markers.

Sorby (1853 p. 145) described the feature now known as *cleavage refraction* in contrasting rocks thus:

> "When slates are composed of alternating beds of different character, the cleavage almost always does not pass straight through them, but lies nearer to the plane of bedding in the fine-grained and more perfectly cleaved varieties. When cleavage cuts the bedding at a moderate angle, this difference is often very considerable; but where the bedding is perpendicular or parallel to it, there is little or no variation."

Sharpe (1849), Sorby (1853) and Harker (1886) had recorded the relationship between slaty cleavage and deformed objects whose principal shortening was perpendicular to cleavage planes. Sorby thus concluded that the refraction of cleavage which he observed (quotation) was a refraction of strain. Harker (1886) described cleavage in terms of a strain ellipsoid and similarly attributed cleavage refraction to refraction of strain ellipsoids, as a consequence of differential volume loss of slate and grit.

This present paper essentially leads on from Sorby and Harker's ideas, but the intervening 130 years of research and debate on the significance of cleavages of various morphologies, to finite strain, cannot be neglected. A review of such work will concentrate on key influences in thinking. For fuller reviews of cleavage, readers are referred to Siddans (1972), Wood (1974), Means (1975, 1977), Tullis (1976), Williams (1976, 1977), White & Knipe (1978), Powell (1979) and Borradaile *et al.* (1982).

A move away from the view that refracting cleavage represented refracting strain was made by Leith (1905, 1914). He introduced the terms 'flow' and 'fracture' cleavage for cleavage observed to refract from slate to sandstone respectively; *flow cleavage* was attributed to flow and recrystallization, and *fracture cleavage* to tensile failure. Leith's two mechanisms of cleavage formation were adhered to by Wilson (1961), and played an important part in subsequent interpretations of cleavage patterns in contrasting lithologies (although questioned by Ramsay 1967). Subsequent explanations of either or both cleavage morphologies arising from *tectonic dewatering* (Maxwell 1962, Powell 1972) were short-lived. However, the two predominant cleavage morphologies remain in use if changed in name to *slaty cleavage* and *spaced cleavage* (Dennis 1967). Spaced cleavages include the genetic terms fracture cleavage, and *pressure solution cleavage* (e.g. Geiser 1974, Gray 1981).

The two commonly observed cleavage morphologies, slaty cleavage and spaced cleavage, may indeed arise from difficent mechanisms. However, they may differ

only on the scale of the *cleavage domains* (Powell 1979, Borradaile *et al.* 1982), or in the relative importance of cleavage-forming processes at the grain scale (rotation, recrystallization and pressure solution of White & Knipe 1978). Moreover, in many rocks there is no clear distinction between two cleavage morphologies, as illustrated by continuous cleavage refraction in graded sedimentary units (e.g. Borradaile *et al.* 1982, p. 515) as described by Ramsay (1967), p. 406).

Despite the continuous spectrum of cleavage morphology observed in rocks, analyses of cleavage with respect to finite strain have been restricted, in the main, to slaty cleavage. The evidence of parallelism of slaty cleavage planes to the $XY$ planes of finite strain ellipsoids ($X > Y > Z$) determined from strained objects and markers, presented by Sharpe (1849), Sorby (1853) and Harker (1886), is supported by subsequent studies (Siddans 1972, Wood 1974). However, Williams (1976, 1977) took a more critical view and in particular questioned the evidence that $XY$ planes are everywhere parallel to slaty cleavage in the North Wales Slate Belt (Tullis & Wood 1975), having observed evidence to the contrary. Such discussions and their answers (Wood & Oertel 1980) are of academic interest, but until data is provided, equal in quantity and accuracy to the evidence in Siddans (1972) and Wood (1974), to demonstrate *consistent non-parallelism* of cleavage to $XY$ planes of strain, the empirical law must remain for slates.

The relationship of finite strain to spaced cleavage is a matter of more controversy. While studies of strain in slates progressed, strain in rocks with spaced cleavage was unsought, perhaps because such cleavages were attributed to fracture or local pressure solution, rather than to finite strain. Recent studies of deformed sandstone dykes associated with spaced cleavage (Geiser 1974, Groshong 1976) seem insufficiently conclusive as proof for or against, parallelism of $XY$ planes to such cleavage. The deformation is very weak, both cleavage and dykes are commonly subperpendicular to bedding, and cleavage–dyke angles small. Whether this suggests an initiation of cleavage perpendicular to bedding and subsequent passive rotation, as the former authors suggest, must await further analyses. It might be asked whether spaced cleavage is a phenomenon of low strain whatever the lithology, or whether it occurs in particular lithologies (e.g. psammitic) which also only develop low strain. The strength of the case for $XY$-plane parallelism to slaty cleavage lies, in part, in the strain intensity which makes for clear $XY$-plane identification in strained objects. If spaced cleavage is a feature of weak strain (even if not parallel to a principal plane) the strain data needed to support or disprove the parallelism of spaced cleavage to local $XY$ planes would require extremely sensitive strain markers and accurate measurement techniques.

Such problems of analyzing the relationship of cleavage to $XY$ planes of finite strain evade the issues of why cleavages should be parallel to $XY$ planes. The reviews of Williams (1976, 1977) and discussion in Hobbs *et al.* (1982) put the case strongly that because cleavage develops through a complexity of microstructural processes (White & Knipe 1978), there would seem no reason to expect cleavage to be parallel to the $XY$ planes of macroscopic strain. The essence of the argument against the parallelism of cleavage and $XY$ planes (Williams 1976, Hobbs *et al.* 1982) is that cleavage, at a particular stage of development, is a *material plane* defined by fabric domains; in contrast the $XY$ plane in a general (rotational) strain history is a *non-material plane*. The authors argued that the two could not remain parallel during progressive strain, unless this was irrotational. However, Ghosh (1982) considered this problem with simple plus pure shear and demonstrated that the angles between initial $XY$-cleavage planes, deformed as passive planes, and finite $XY$ planes was less than 5° and thus probably not measurable. Whether this argument applies to material and non-material planes in layers with very low strain, where spaced cleavages occur, awaits confirmation.

In contrast with the above school of thought is that led by Ramsay (1967), which holds that cleavage patterns are natural finite-strain trajectories. The similarity between *cleavage fans* around natural folds (Mukhopadhay 1965, Roberts 1971), and strain patterns in experimental folds (Ramberg 1962, Roberts & Strömgård 1972) is given as evidence for the assumption that all cleavages are subparallel to $XY$ planes. Ramsay (1967, pp. 403–406) discussed cleavage refraction and cleavage fanning around folds together, in terms of models of strain in folding: cleavages fans were described as convergent or divergent with respect to an anticlinal fold. Thus cleavage refraction would be part of a cleavage-fanning system as a result of folding. Finite element analyses of folds (Dieterich & Carter 1969, Shimamoto & Hara 1976) afford a comparison of strain patterns in theoretical folds with natural cleavage patterns (Dieterich 1969). The similarity of the patterns has confirmed the view that natural cleavages are parallel to $XY$ planes of finite strain. The mechanical problems of cleavage formation do not enter this line of argument.

In the present paper, cleavage refraction is considered as a feature peculiar to a change of lithology rather than dependent on a particular form of strain in folding. The manner of cleavage refraction described by Sorby (1853, quoted previously) and Harker (1886) will be investigated in the following way: given a particular strain state in one rock type, what would be a compatible strain state in an adjacent rock type of different properties? To answer this, a theoretical model of finite strain variation through layers of contrasting properties is developed which is considered applicable to rocks, following earlier infinitesimal strain refraction theories (Treagus 1973, 1981). This approach is distinct from Goguel's (1982) which used slaty-cleavage refraction to derive stress patterns in contrasting lithologies by assuming that cleavage formed perpendicular to a principal stress.

Strain patterns derived theoretically in the present paper will be applied to geological strain variations, and compared to observed cleavage refraction patterns. The similarities, or differences, of strain refraction patterns (particularly the sense of refraction with associated strain variations), and natural cleavage refraction pat-

terns and cleavage morphology changes, should contribute to the debate on the relationships between cleavage and strain.

## THEORETICAL MODEL OF TWO-DIMENSIONAL FINITE STRAIN REFRACTION

A two-dimensional geometrical model of strain refraction is shown in Fig. 1(a). Two strain ellipses of different shape but equal areas in layers A and B, meet at the layer interface trace, $x$. Thus the two longitudinal strains along $x$ are equal for A and B, but the shear strains are not. The two semiellipses are geometrically compatible, but an infinite number of compatible ellipses could be drawn for B (Fig. 1b). It is common in geology to use geometric or kinematic models for structures (e.g. Hobbs 1971), but the disadvantage is that such models may not be viable dynamically. In the case of strain-ellipse refraction, criteria are required to distinguish which of the configurations in Fig. 1(b) is mechanically viable: it is assumed there is only one solution for a particular AB system.

The criteria used in the theory follow those of two previous studies (Treagus 1973, 1981) of infinitesimal strain refraction in viscous layers. The system is defined in Fig. 2 and the assumptions and constraints of continuity are listed below.

(1) The material of layers A and B are Newtonian viscous throughout deformation with homogeneous viscosities of $\eta_A$ and $\eta_B$ respectively and viscosity ratio $V = \eta_B/\eta_A$.

(2) The materials are incompressible so the strain ellipsoid axes ($X > Y > Z$) have the relationship $X_A \cdot Y_A \cdot Z_A = X_B \cdot Y_B \cdot Z_B = 1$.

(3) The interface plane ($xz$) of layer A to layer B contains one principal axis of strain ellipsoids A and B. Unless otherwise defined this is $Y$, the two-dimensional view is the $XZ$ plane of each ellipsoid, and $Y_A = Y_B$.

(4) For initial simplicity, plane strain is assumed such that $Y_A = Y_B = 1$. Modifications will be applied in subsequent sections.

(5) The strain ellipse on the interface plane ($xz$) is the same for A and B. In terms of quadratic elongations, $\lambda_{Ax} = \lambda_{Bx}$, and reciprocals $\lambda'_{Ax} = \lambda'_{Bx}$. Similarly, $\lambda_{Az} = \lambda_{Bz}$ and $\lambda'_{Az} = \lambda'_{Bz}$; from (4) these would be unity.

(6) The condition of contact is that the shear stress parallel to $x$ is equal for A and B, throughout the strain history: $\tau_{Ax} = \tau_{Bx}$. Hence $\eta_A\dot{\gamma}_{Ax} = \eta_B\dot{\gamma}_{Bx}$, where $\dot{\gamma}$ is the infinitesimal shear-strain rate. The relationship of finite shear strain is found to be simply $\eta_A\gamma_{Ax} = \eta_B\gamma_{Bx}$ or $\gamma_{Ax}/\gamma_{Bx} = V$ (see Appendix 1). [This simple equation is also derived (for the Newtonian case but not for other rheological models) in a parallel study of the kinematics and mechanics of interfaces by Cobbold (this issue)].

Denoting $\gamma' = \gamma/\lambda$ (Ramsay 1967, p. 68) it follows that $\gamma'_{Ax}/\gamma'_{Bx} = V$ also.

Of these six criteria, the last two are particular constraints of this model which arise from assumptions of continuity and adherence. The equations can be combined to give an algebraic solution for finite strain refraction across a viscosity contrast of known ratio and orientation. The full algebraic solution is given in Appendix 2. The key equations needed for the reader to determine solutions for particular systems are given in Table 1.

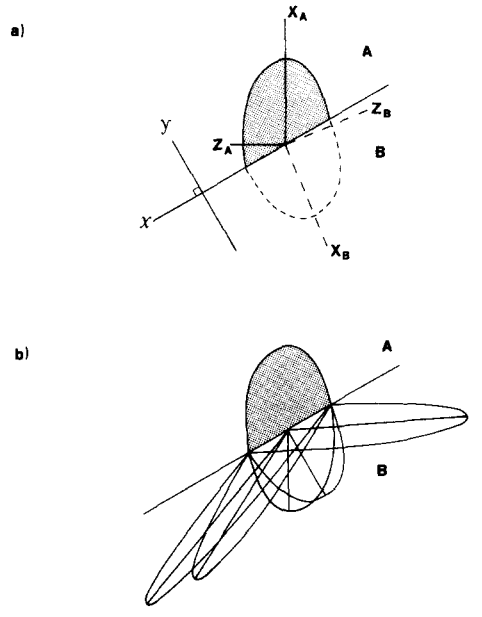


Fig. 1. (a) A geometrical model of strain refraction. (b) A series of geometrically-viable refracted strain ellipses in B from a known ellipse (A).

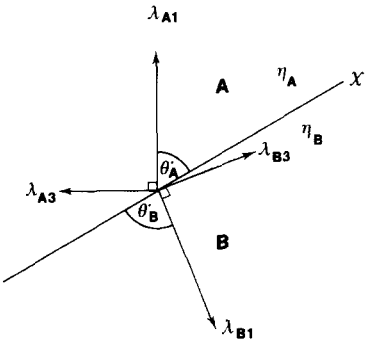


Fig. 2. Theoretical model with nomenclature; $x$ is the interface trace of plane $xz$ between layers A and B.

Table 1. Summary of algebraic solution, from Appendix.

$\lambda'_{A1}$, $\theta'_A$ and $V$ $(=\eta_B/\eta_A)$ are known variables defined in Fig. 2. Calculate

$$L = \lambda'_{Ax} = \frac{(1 + \lambda'^2_{A1}) - (1 - \lambda'^2_{A1})\cos 2\theta'_A}{2\lambda'_{A1}}$$

$$S = \gamma'_{Ax} = \frac{(1 - \lambda'^2_{A1})\sin 2\theta'_A}{2\lambda'_{A1}}$$

$$M = \frac{1 + L^2 + S^2/V^2}{L}.$$

Then

$$\lambda'_{B1} = \frac{M - \sqrt{M^2 - 4}}{2}$$

$$\lambda'_{B3} = \frac{M + \sqrt{M^2 - 4}}{2} = 1/\lambda'_{B1}$$

$$\theta'_B = \frac{\sin^{-1}[2S/(V\sqrt{M^2 - 4})]}{2}, \text{ or}$$

$$\theta'_B = \tan^{-1}[2SLV/(V^2 - V^2L^2 + S^2)]/2.$$

Solutions may be obtained without such computation, however, but by Mohr construction. This method not only provides graphical solutions to the equations in Table 1, but also serves as a useful tool to illustrate the theoretical framework.

*The Mohr diagram as a graphical solution*

The Mohr diagram for reciprocal quadratic elongation will be used, following Ramsay (1967, p. 73). The method is illustrated by the example in Fig. 3. Circles are drawn for the states of strain in two dimensions (plane $xy$, Fig. 1a); these are the $XZ$ principal planes. It is assumed that $\lambda'_{A1}$, $\lambda'_{A3}$ and $\theta'_A$ are known. Using $2\theta'_A$, the coordinates of $x_A$ ($\lambda'_{Ax}$, $\gamma'_{Ax}$) will define $L$ and $S$, respectively. From laws (5) and (6) above $\lambda'_{Bx} = \lambda'_{Ax}$ and $\gamma'_{Bx} = \gamma'_{Ax}/V$. Hence, the coordinates of $x$ for layer B ($x_B$) are $L$ and $S/V$. In Fig. 3, $V = 0.5$ and $x_B$ is plotted accordingly. One point on the Mohr circle for layer B is therefore known.

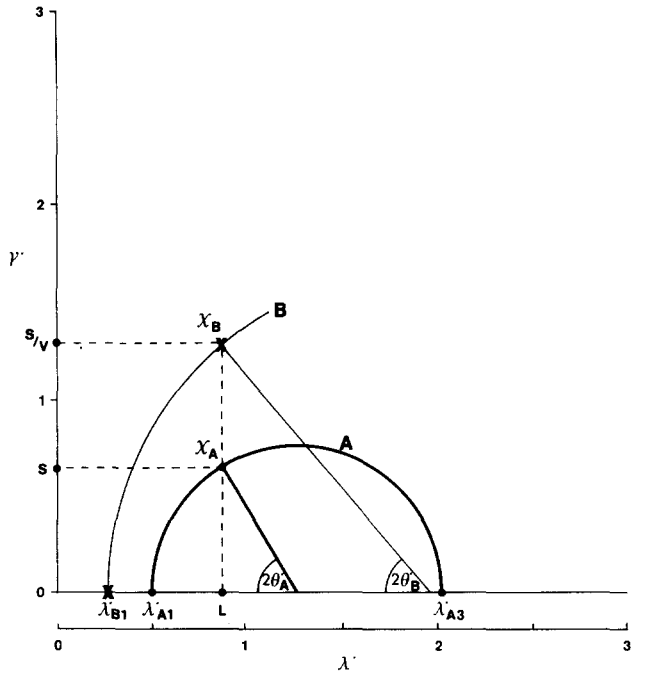


Fig. 3. The Mohr diagram method of strain solution—see text for explanation.

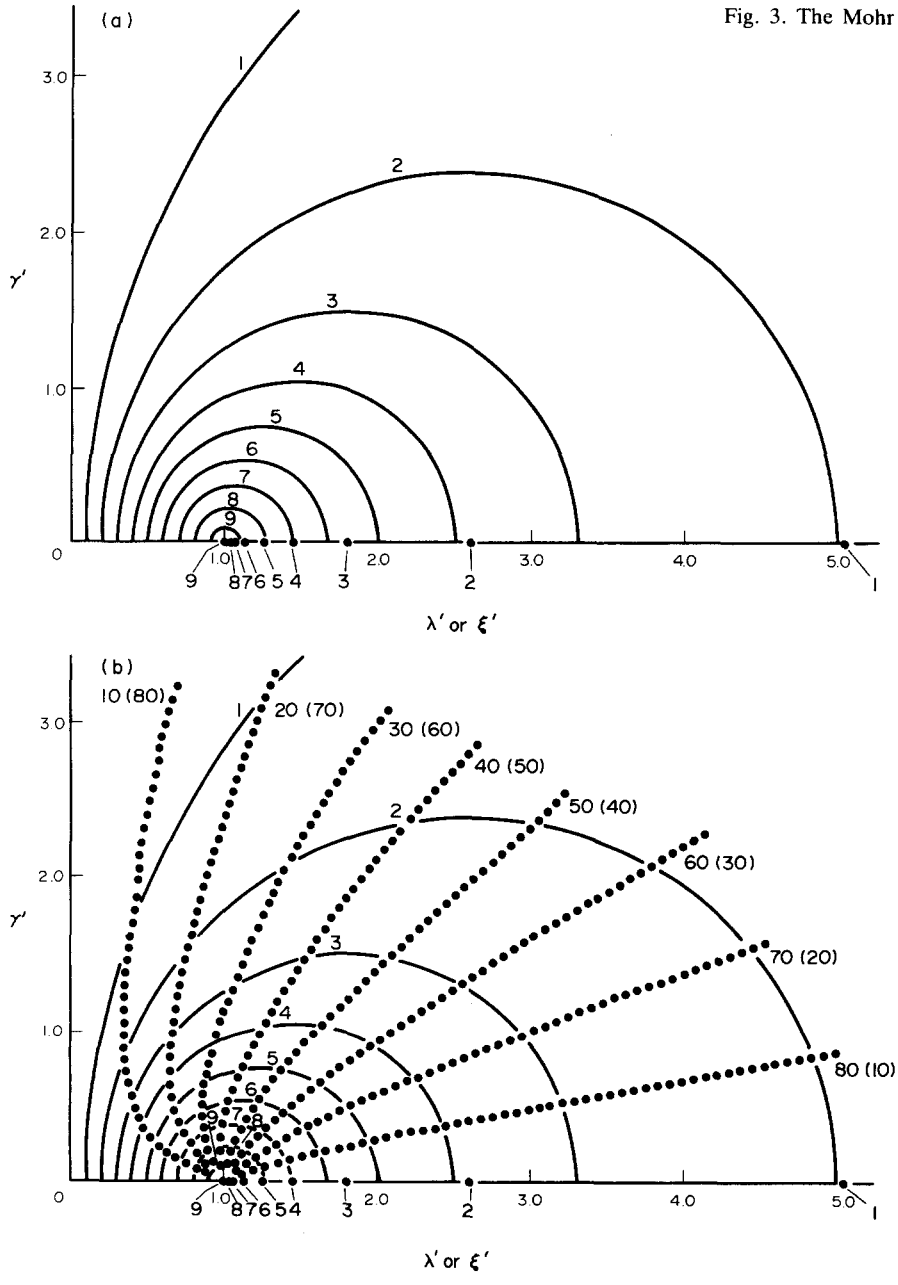


The assumption of plane strain such that $\lambda'_{A1} \cdot \lambda'_{A3} = \lambda'_{B1} \cdot \lambda'_{B3} = 1$ also limits the position of the Mohr circle. There is a unique set of circles which may be drawn for this condition, shown in Fig. 4. The position of $x_B$ plotted on Fig. 4 will immediately give the Mohr circle for B: it has $\lambda'_{B1} = 0.27$, $\lambda'_{B3} = 3.7$ and $\theta'_B = 25°$.

The Mohr-diagram method may be used to derive all solutions for refracted strains for layers A to B, on one figure. The Mohr circle for layer A represents strain in any orientation in the $xy$ plane, so represents all $\theta'_A$ (double angles clockwise). Compatible strains in B fall on an ellipse of distortion proportional to the inverse of $V$ (Fig. 5). Individual Mohr circles can be drawn from points on this elliptical locus, using the contours of Fig. 4. Figure 5, therefore, completely illustrates the control of the viscosity ratio on refracted strains, particularly the large strains generated in layers of relatively low viscosity; it illustrates which orientations of layering ($x$) generate maximum and minimum strains in B.

Fig. 4. Sets of Mohr circles satisfying the conditions of equal-area plane strain ($\lambda'$) or equal-area apparent plane strain ($\xi'$). Numbered dots on the abcissae are the centres of each numbered Mohr circle. The dotted loci in (b) join points of equal $\theta'_B$ (numbered): the complementary angles in brackets are equivalent to the strain angle $\beta_s$ of Treagus (1982).

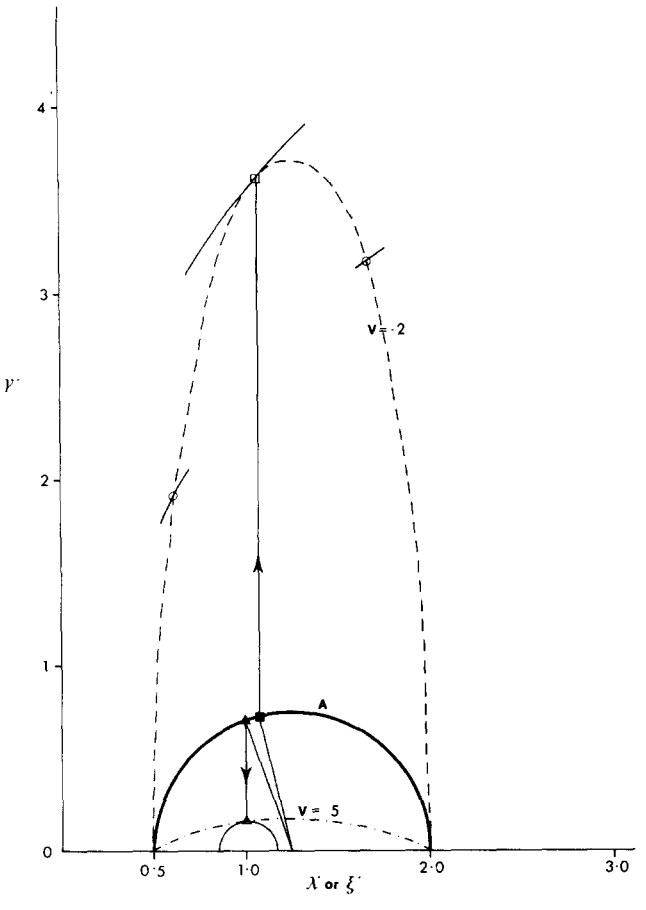


Fig. 5. Mohr diagram showing Mohr circle A distorted according to viscosity ratio $V$ (numbered). The position for minimum refracted strain is given by the triangle–triangle arrow to the $V = 5$ locus and the appropriate Mohr strain circle drawn. Similarly the position of maximum refracted strain is given by the square–square arrow to the $V = 0.2$ locus, and part of the appropriate Mohr strain circle drawn. The two circles on the $V = 0.2$ locus indicate positions, on the apparent plane strain Mohr diagram ($\xi'$, $\gamma'$), of pure construction ($k = \infty$) for $XY$ planes and pure flattening ($k = 0$) for $YZ$ planes: these are discussed later under "Strain refraction of other principal planes".

## STRAIN REFRACTION RESULTS, PLANE STRAIN

The theory and its Mohr-diagram method of solution will be illustrated by four examples (Fig. 6). As formerly defined, the plane of study ($xy$ plane, Fig. 1a) is the $XZ$ principal plane, and $Y_A = Y_B = 1$ is parallel to $z$ on the interface plane. A state of strain is chosen for A to be the same in the four examples of Fig. 6: $\lambda'_{A1} = 0.5$, $\lambda'_{A3} = 2.0$; that is $X_A = 1.41$, $Y_A = 1$, $Z_A = 0.71$. Two viscosity ratios of $V = 5$ and $V = 0.2$ ($V = \eta_B/\eta_A$) and two $\theta'_A$ interface orientations ($x \wedge X_A$) of 60° and 30° are chosen. The Mohr-diagram solutions are accompanied by the actual $XZ$ strain ellipses for A and B in Figs. 6(a)–(d). Exact results are given in Table 2.

The results of Fig. 6 demonstrate the control of viscosity ratio $V$, and interface orientation $\theta'_A$, on the size and orientation of the refracted strain ellipses in B. Figures 6(a) & (b) for the more viscous 'layer' than A, ($V = 5$) show B ellipses nearer to circular than A ellipses; that is, lower strain values. The refraction of the strain axes is towards orthogonal to the interface. In Fig. 6(a), $X_B$ is closer to the interface pole, but in Fig. 6(b) $Z_B$ is refracted towards this pole. Thus, the orientation of the interface ($\theta'_A$) controls the sense of refraction in the $V > 1$ examples.

Figures 6(c) and (d) show refracted strains in the less viscous 'layer' than A, ($V = 0.2$). In both examples high-value strains occur. The sense of refraction does not change with $\theta'_A$: for both (c) and (d), $X_B$ lies closer to the interface trace than $X_A$ so that $\theta'_A > \theta'_B$. With increasing B strain, $\theta'_B$ reduces to quite small angles. Because the strain in $x$ is low compared to the principal strains, the B strain ellipse (incompetent) may be approximated to simple shear in $x$. However good the approximation, it is merely a geometric one; only where $x$ is a line of no-finite-longitudinal-strain in ellipse A, can the B ellipses be truly termed simple-shear ellipses.

The above examples have limited application, but are useful for illustration. The Mohr-diagram method may be used to derive data on a more varied system of viscosity ratios and layer orientations, and in different states of reference strain (A). Following the method of Fig. 5, Fig. 7 shows strain loci for two values of $\lambda'_{A1}$ (0.5 and 0.25) and six viscosity ratios in the range 0.1–10. Figure 7(a) may be used in conjunction with the contoured diagram (Fig. 4) assuming equal-area plane strain, to give specific values of $\theta'_B$ and $\lambda'_{B1}$ for particular $\theta'_A$ and $V$. Likewise, Fig. 7(b) may be used with a similar contoured diagram at the appropriate scale. Values of $\lambda'_{B1}$ have been converted to shortening $Z_B$, and the results graphed against reference orientation $\theta'_A$ in Fig. 8. Maximum variations of $Z_B$ from $Z_A$ occur in the range $\theta'_A = 30$–$50°$ in both graphs.

Figure 9 illustrates angles of strain refraction: (a) is for infinitesimal strain (from Treagus 1973) and (b) and (c) for the two reference strain states ($\lambda'_{A1} = 0.5$ and 0.25) in Figs. 7 and 8. The angle of strain refraction is the difference ($\theta'_A$–$\theta'_B$); this is given in Fig. 9 by the ordinate distance from the diagonal line $\theta'_A = \theta'_B$, simply measured on the $\theta'_B$ scale. Where curves cross the diagonal line are positions of no refraction and therefore homogeneous strain of A and B. Figure 9 may be used to construct strain trajectories through contrasting viscous

Table 2. Numerical results for plane-strain examples, $Y$ parallel to layering

| $X_A$ | $Y_A$ | $Z_A$ | $\lambda'_{A1}$ | $\lambda'_{A3}$ | $V$ | $\theta'_A$ | : | $\lambda'_{B1}$ | $\lambda'_{B3}$ | $X_B$ | $Y_B$ | $Z_B$ | $\theta'_B$ |
|---|---|---|---|---|---|---|---|---|---|---|---|---|---|
| 1.41 | 1.0 | 0.71 | 0.5 | 2.0 | 5.0 | 60° | : | 0.61 | 1.64 | 1.28 | 1.0 | 0.78 | 83° |
| ,, | ,, | ,, | ,, | ,, | ,, | 30° | : | 0.83 | 1.21 | 1.1 | 1.0 | 0.91 | 20° |
| ,, | ,, | ,, | ,, | ,, | 0.2 | 60° | : | 0.12 | 8.62 | 2.94 | 1.0 | 0.34 | 25° |
| ,, | ,, | ,, | ,, | ,, | ,, | 30° | : | 0.07 | 14.0 | 3.75 | 1.0 | 0.27 | 14° |

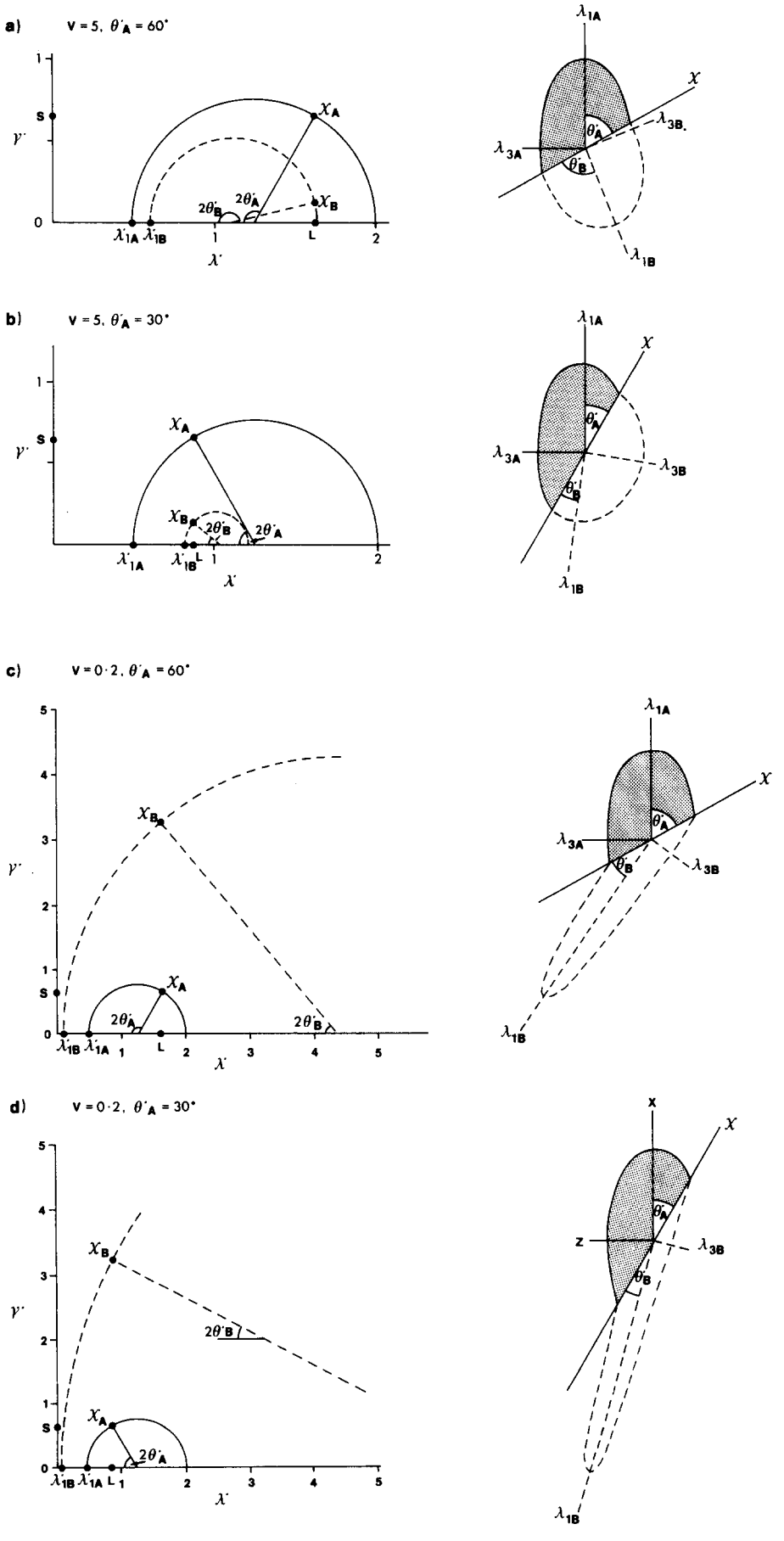


Fig. 6. Mohr-diagram solution and strain-ellipse sketches, for four examples of $Y = 1$ parallel to layering and $\lambda'_{A1} = 0.5$: (a) $V = 5$, $\theta'_A = 60°$; (b) $V = 5$, $\theta'_A = 30°$; (c) $V = 0.2$, $\theta'_A = 60°$; (d) $V = 0.2$, $\theta'_A = 30°$.

layers. Figure 10 shows the $X$ trajectories (the $XY$ plane traces) for two layering orientations: trace 1 is the infinitesimal $X$ trajectory and traces 2 and 3 $X$ trajectories for different finite reference strain states in the shaded layers. Associated with the angular strain refraction is a progressive increase in strain intensity with a decrease in $V$, shown in Fig. 8.

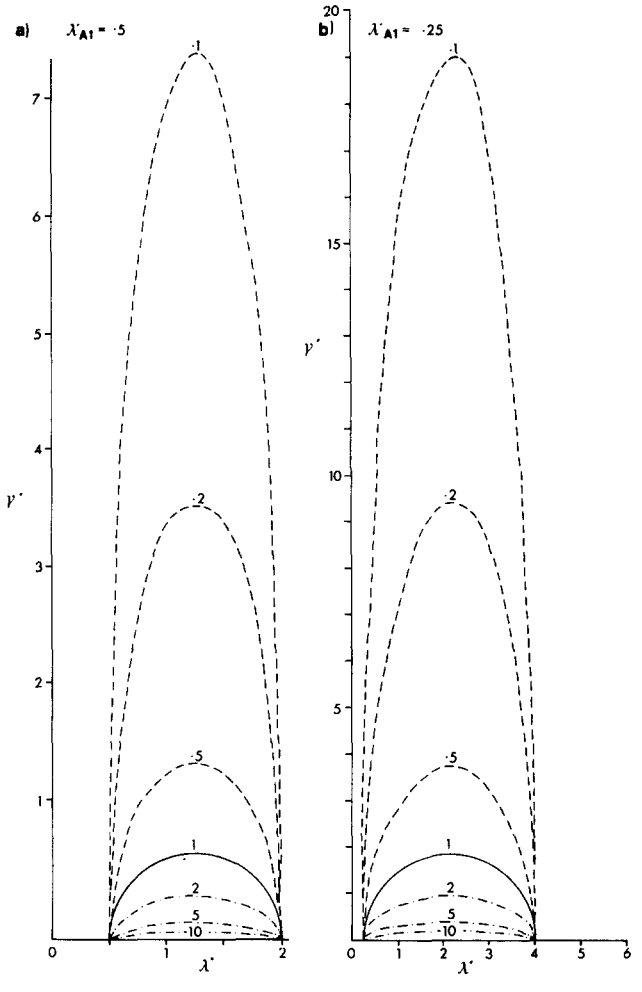


Fig. 7. Mohr-diagram loci (see Fig. 5) for viscosity ratios $V = 0.1, 0.2, 0.5, 2, 5$ and 10 (numbered): (a) reference strain $\lambda'_{A1} = 0.5$ ($X_A = 1.41, Z_A = 0.71$); (b) $\lambda'_{A1} = 0.25$ ($X_A = 2.0, Z_A = 0.5$).

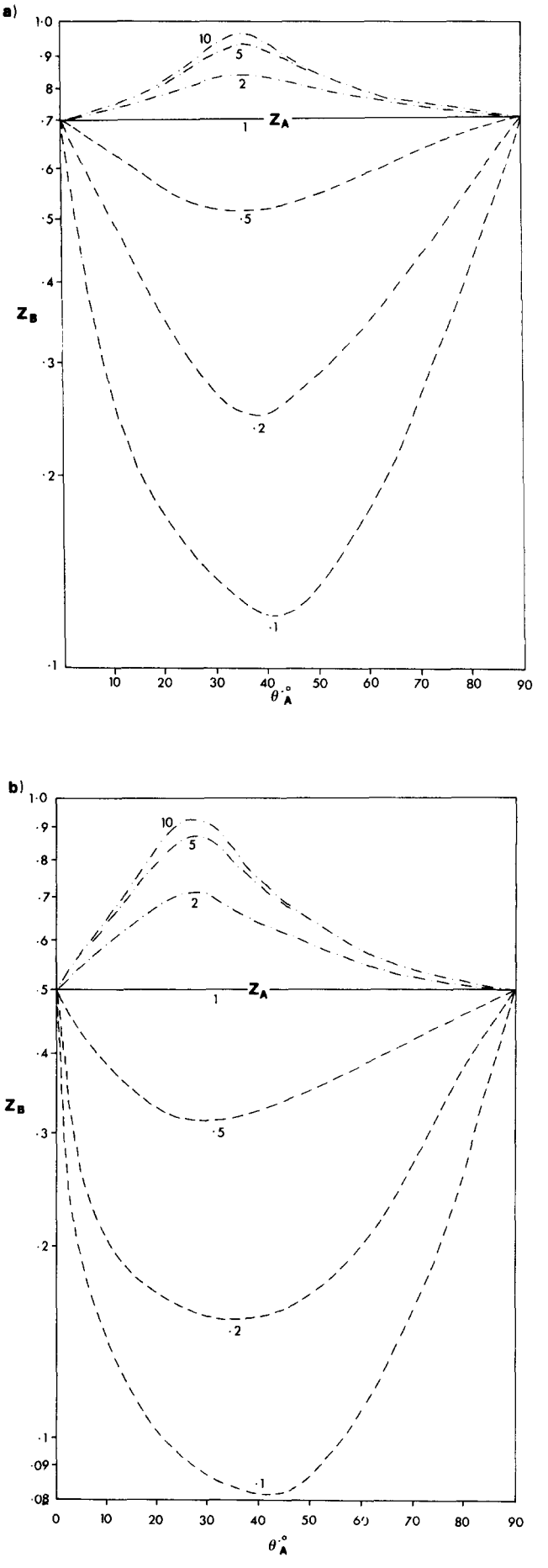


Fig. 8. Values of refracted strain (taken from Fig. 7), graphed against $\theta'_A$ and given as $Z_B$ ($=\lambda'^{1/2}_{B1}$): (a) $Z_A = 0.71$; (b) $Z_A = 0.5$; $V$ as numbered.

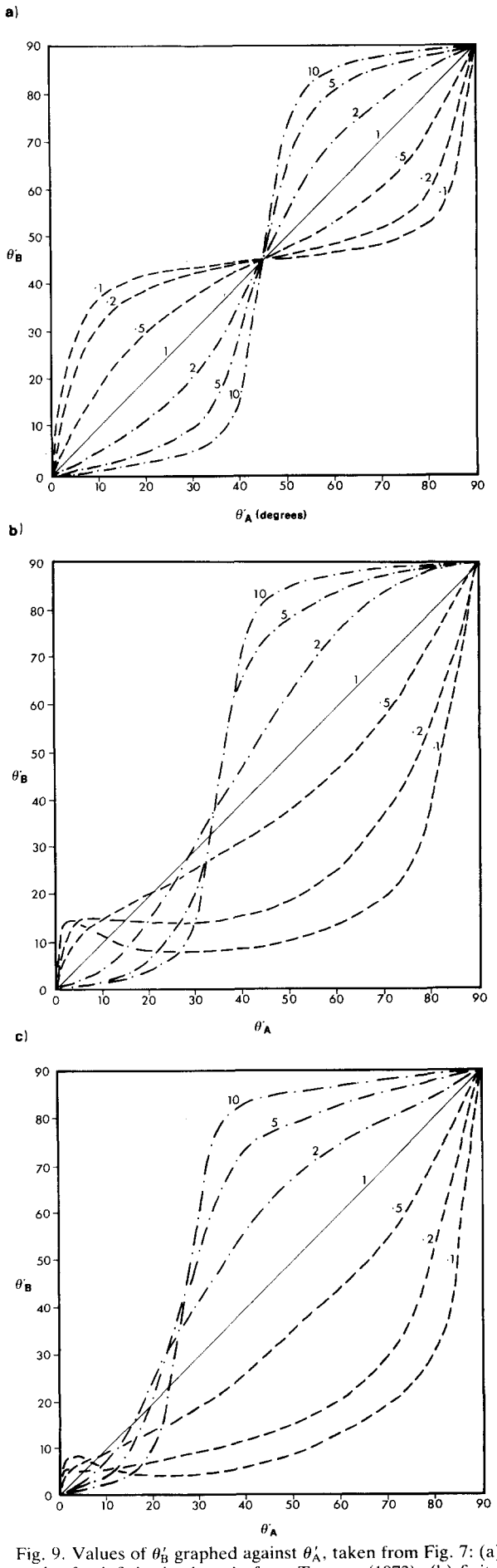


Fig. 9. Values of $\theta'_B$ graphed against $\theta'_A$, taken from Fig. 7: (a) strain angles for infinitesimal strain from Treagus (1973); (b) finite strain angles, $Z_A = 0.71$; (c) finite strain angles, $Z_A = 0.5$.

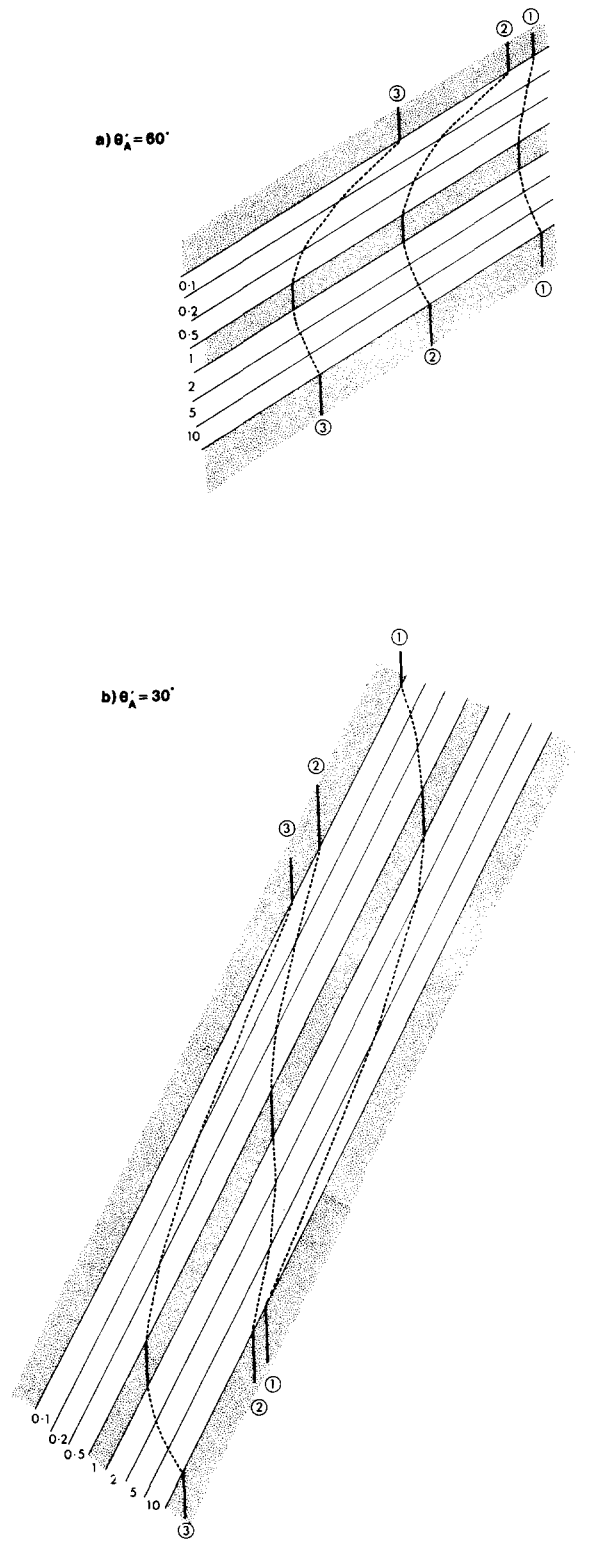


Fig. 10. Three strain trajectories ($X$) in multilayers of varied viscosity ratio $V$ (numbered) to the reference layer (shaded); data taken from Fig. 9. Trace 1 is the infinitesimal $X$ trajectory after Treagus (1973), (Fig. 9a); trace 2 is the $X$ trajectory for reference strain $X_A = 1.41$, $Z_A = 0.71$ (Fig. 9b); trace 3 is the $X$ trajectory for reference strain $X_A = 2.0$, $Z_A = 0.5$ (Fig. 9c). $Y = 1$ parallel to layering, perpendicular to page throughout. (a) $\theta'_A = 60°$ and (b) $\theta'_A = 30°$.

## STRAIN REFRACTION RESULTS FOR NON-PLANE-STRAIN ELLIPSOIDS

The theory so far presented has been for two-dimensional strain refraction where the plane of study, $xy$ of the model, is the $XZ$ principal plane of all strain ellipsoids, $Y=1$ and thus $X=1/Z$. It was the last condition which made the Mohr diagram method so simple (Fig. 4). It is possible to extend the theory to non-plane-strain ellipsoids ($Y_A = Y_B \neq 1$) and still obtain solutions. In this case ellipse $X_AZ_A$ and ellipse $X_BZ_B$ are not unit area ellipses, but have areas $1/Y_A$ if deformation is volume conservative.

A method is used where the $XZ$ strain ellipses are treated as apparent unit-area ellipses by altering the scale. For example, ellipse A may be scaled such that the axes $X_A$ and $Z_A$ are both multiplied by a factor $1/Y_A^{1/2}$ and the scaled axes then have a reciprocal relationship. Ellipse B must be scaled accordingly. The apparent-unit-area ellipse A may be plotted on the Mohr unit-area contoured diagram (e.g. Fig. 4), the apparent ellipse B obtained from $V$, and the real strain ellipse B determined by scaling back.

The symbol $\xi'$ will be used for reciprocal quadratic elongations in the apparent unit-area strain ellipses. In layer A, $\lambda'_{A1} = 1/X_A^2$, $\lambda'_{A2} = 1/Y_A^2$ and $\lambda'_{A3} = 1/Z_A^2$. Hence $\xi'_{A1} = \lambda'_{A1}/Y_Z$ or $\xi'_{A1} = 1/X_A^2 \cdot Y_A$ and $\xi'_{A3} = 1/Z_A^2 \cdot Y_A$. Similarly in layer B, $\xi'_{B1} = 1/X_B^2 \cdot Y_B$ and $\xi'_{B3} = 1/Z_B^2 \cdot Y_B$ and $Y_A = Y_B$.

For simplicity, examples are considered here where the apparent unit area strain ellipse has $\xi'_{A1} = 0.5$, $\xi'_{A3} = 2.0$ so that the apparent strain ellipses are identical in shape to the real strain ellipses in Fig. 6 and Table 2. Four examples of $Y_A$ are considered for each, and the apparent and real refracted strain results given in Table 3. The value of $Y_A$ does not affect $\theta'_B$ but it affects the absolute strain. In all the examples the ellipsoids are triaxial, and may best be compared in size and shape on a Flinn (1962) style plot (Fig. 11). The strain ellipsoids in the $V = 5$ layers fall into a low strain area with $k$ ranging from 0 to $\infty$. Positions where loci are reflected at the graphical coordinates indicate an interchange in strain axes from A to B such that $Y_A = X_B$ or $Y_A = Z_B$ (starred in Table 3). In these cases the two-dimensional

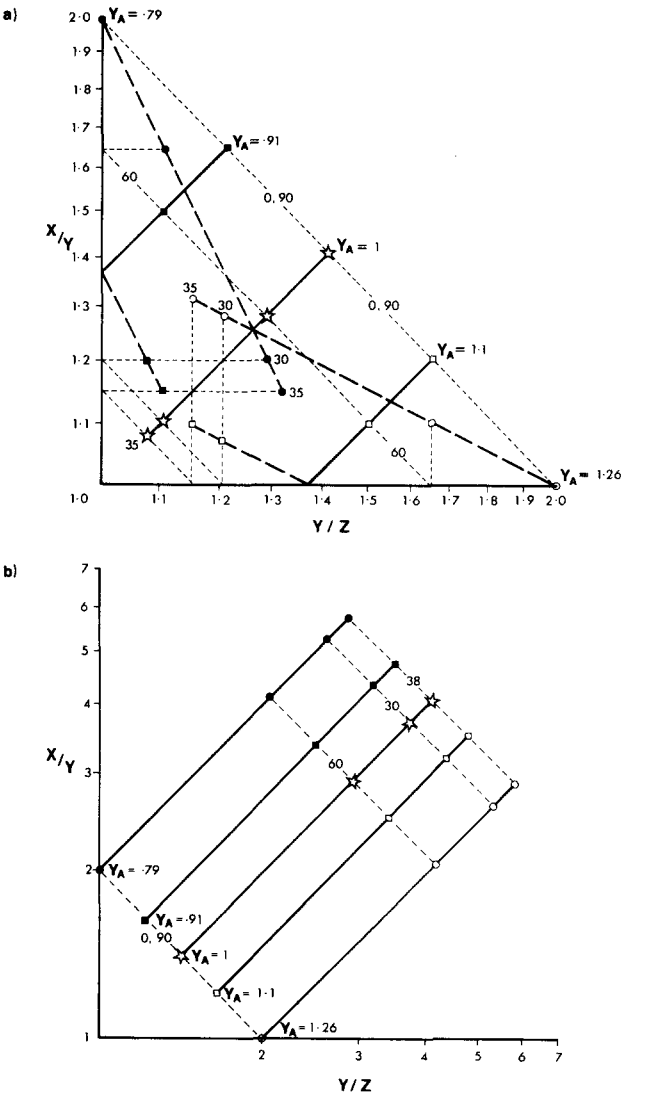


Fig. 11. Flinn (1962)-type strain plots of $X/Y$ against $Y/Z$, logarithmic scale for non-plane-strain examples of Table 3. Examples where $V = 5$ are plotted in (a) and $V = 0.2$ in (b); note the different scales. For all examples $\xi'_{A1} = 0.5$. Loci of strain refraction for a particular $Y_A$ (numbered) and variable $\theta'_A$ are given by heavy lines with symbols, shown broken in the axial-interchange mode. Loci of strain refraction for a particular $\theta'_A$ (degrees numbered 30, 60, etc.) and variable $Y_A$ are marked by fine pecked lines. The refracted strain ellipsoids for Fig. 6 are shown by stars where the $Y_A = 1$ locus intersects the $\theta'_A = 30$ and 60° loci.

Table 3. Numerical results for non-plane-strain examples, $Y$ parallel to layering

| $X_A$ | $Y_A$ | $Z_A$ | $\xi'_{A1}$ | $\xi'_{A3}$ | $V$ | $\theta'_A$ | : | $\xi'_{B1}$ | $\xi'_{B3}$ | $X_B$ | $Y_B$ | $Z_B$ | | $\theta'_B$ |
|---|---|---|---|---|---|---|---|---|---|---|---|---|---|---|
| 1.26 | 1.26 | 0.63 | 0.5 | 2.0 | 5.0 | 60° | : | 0.61 | 1.64 | 1.26 | 1.14 | 0.7 | * | 83° |
| ,, | ,, | ,, | ,, | ,, | ,, | 30° | : | 0.83 | 1.21 | 1.26 | 0.98 | 0.81 | * | 20° |
| ,, | ,, | ,, | ,, | ,, | 0.2 | 60° | : | 0.12 | 8.62 | 2.57 | 1.26 | 0.30 | | 25° |
| ,, | ,, | ,, | ,, | ,, | ,, | 30° | : | 0.07 | 14.0 | 3.37 | 1.26 | 0.24 | | 14° |
| 1.22 | 1.1 | 0.74 | 0.5 | 2.0 | 5.0 | 60° | : | 0.61 | 1.64 | 1.22 | 1.1 | 0.74 | | 83° |
| ,, | ,, | ,, | ,, | ,, | ,, | 30° | : | 0.83 | 1.21 | 1.1 | 1.04 | 0.86 | * | 20° |
| ,, | ,, | ,, | ,, | ,, | 0.2 | 60° | : | 0.12 | 8.62 | 2.75 | 1.1 | 0.33 | | 25° |
| ,, | ,, | ,, | ,, | ,, | ,, | 30° | : | 0.07 | 14.0 | 3.6 | 1.1 | 0.25 | | 14° |
| 1.49 | 0.91 | 0.75 | 0.5 | 2.0 | 5.0 | 60° | : | 0.61 | 1.64 | 1.35 | 0.91 | 0.82 | | 83° |
| ,, | ,, | ,, | ,, | ,, | ,, | 30° | : | 0.83 | 1.21 | 1.16 | 0.96 | 0.91 | * | 20° |
| ,, | ,, | ,, | ,, | ,, | 0.2 | 60° | : | 0.12 | 8.62 | 3.03 | 0.91 | 0.35 | | 25° |
| ,, | ,, | ,, | ,, | ,, | ,, | 30° | : | 0.07 | 14.0 | 3.96 | 0.91 | 0.28 | | 14° |
| 1.60 | 0.79 | 0.79 | 0.5 | 2.0 | 5.0 | 60° | : | 0.61 | 1.64 | 1.42 | 0.88 | 0.79 | * | 83° |
| ,, | ,, | ,, | ,, | ,, | ,, | 30° | : | 0.83 | 1.21 | 1.23 | 1.02 | 0.79 | * | 20° |
| ,, | ,, | ,, | ,, | ,, | 0.2 | 60° | : | 0.12 | 8.62 | 3.33 | 0.79 | 0.39 | | 25° |
| ,, | ,, | ,, | ,, | ,, | ,, | 30° | : | 0.07 | 14.0 | 4.20 | 0.79 | 0.30 | | 14° |

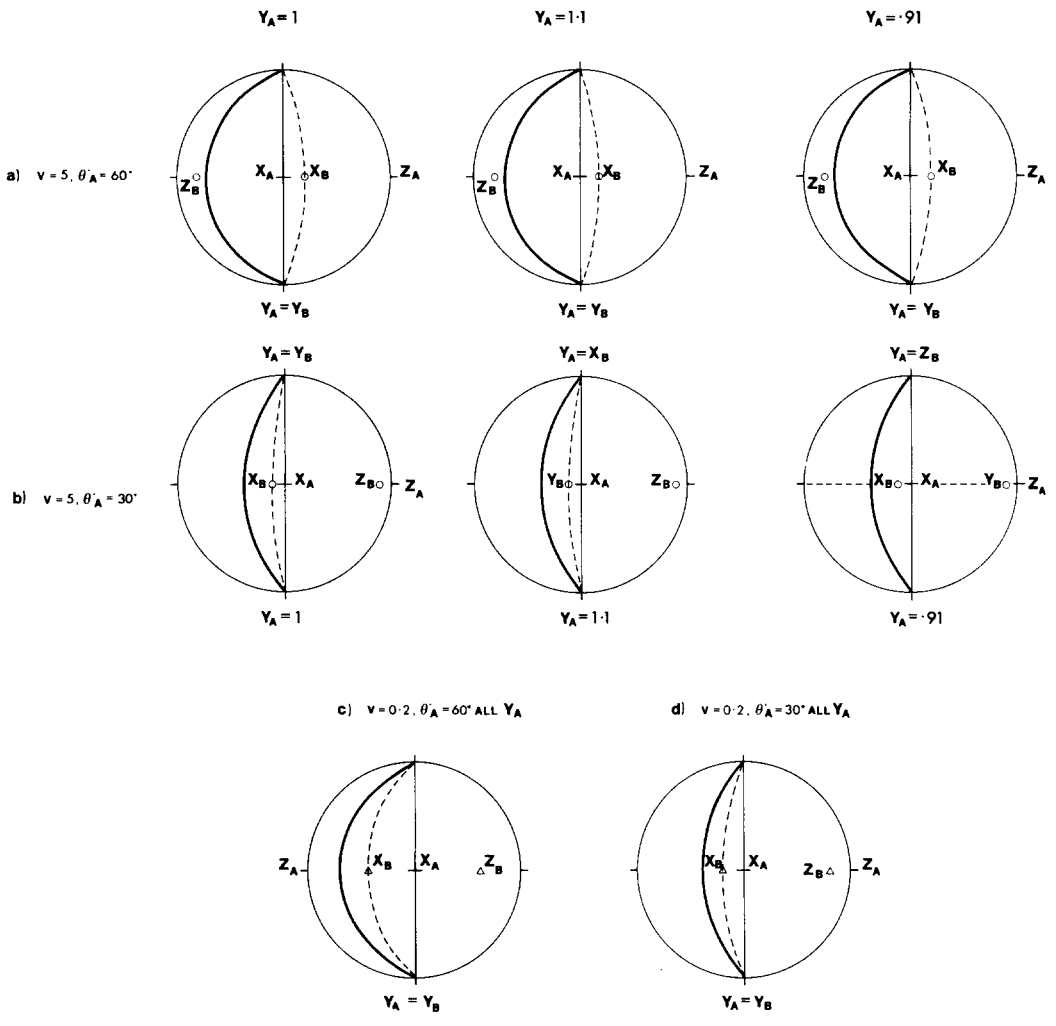


Fig. 12. Orientations of refracted strain axes in examples of varied $Y_A$ value parallel to layering (Table 3), and with strain ellipsoid shapes shown in Fig. 11. For all examples $\xi'_{A1} = 0.5$. Heavy lines show the interface trace, pecked lines the refracted $XY$ planes. Note axial interchange in (b) for $Y_A = 1.1$ and 0.91. (Lower hemisphere equal-area nets.)

plane of study changes from $XZ$ in A to $YZ$ or $XY$ in B. In contrast the strain ellipsoids in the $V = 0.2$ layers (Fig. 11b) show no instances of axial interchange but consistently high strain, reaching a maximum for $\theta'_A = 38°$.

The orientations of $X_B$, $Y_B$ and $Z_B$ are illustrated stereographically for the examples in Table 3, in Fig. 12. The normal sense of strain axes occurs in plots (a), (c) and (d), but (b) shows axial interchange.

## STRAIN REFRACTION RESULTS FOR OTHER PRINCIPAL PLANES

The two-dimensional finite strain refraction theory has, until now, been restricted to $Y_A = Y_B$ parallel to layering and to the $XZ$ plane as the plane of study. It is possible to apply the theory to the other principal planes, however. The two-dimensional theory merely requires one principal axis of the strain ellipsoid to parallel layering, and this may be $X$ or $Z$ as well as $Y$. The apparent plane-strain method of the previous section will be followed.

### XY *principal planes*

In this case $Z_A = Z_B$ is parallel to $z$ in layering. The $X_AY_A$ and $X_BY_B$ strain ellipses will have areas $1/Z_A$. They may be converted to apparent unit-area ellipses of reciprocal quadratic elongations $\xi'$ by $\xi'_{A1} = 1/X_A^2 \cdot Z_A$, $\xi'_{A2} = 1/Y_A^2 \cdot Z_A$ and similarly for layer B.

Examples are again considered which make use of the results in Fig. 5: $\xi'_{A1} = 0.5$, $\xi'_{A2} = 2.0$, and $V = 5$ or 0.2. $Y_A$ is here taken as unity. The real and apparent strain for layer A, and the results for layer B are given in Table 4. The strain plot (Fig. 13) illustrates the change in $k$ value from $k = 1$ in A to various B values. The $V = 5$ line (solid) shows refracted strain ellipsoids move into the flattening field with increasing $\theta'_A$, to the most oblate form at $\theta'_A = 35°$ (this is the minimum strain shown by the solid triangle of Fig. 5); from $\theta'_A = 35$–$90°$ the ellipsoids move back to $k = 1$. The $V = 0.2$ lines (broken) in Fig. 13 indicate strain ellipsoids in the prolate field with critical angles of $\theta'_A = 15$ and 61° where the strain is pure constriction ($k = \infty$, $Y_B = Z_B$). These strain states are indicated in Fig. 5 (circles) by the points where the Mohr circle for $\xi'_{B1} = 0.5^{1/3}$ cuts the elliptical locus labelled $V = 0.2$. In the field $\theta'_A = 15$–61°, there is an inter-

Table 4. Numerical results for $XY$-plane solutions, $Z$ parallel to layering

| $X_A$ | $Y_A$ | $Z_A$ | $\xi'_{A1}$ | $\xi'_{A2}$ | $V$ | $\theta'_A$ | : | $\xi'_{B1}$ | $\xi'_{B2}$ | $X_B$ | $Y_B$ | $Z_B$ | $\theta'_B$ |
|---|---|---|---|---|---|---|---|---|---|---|---|---|---|
| 2.0 | 1.0 | 0.5 | 0.5 | 2.0 | 5.0 | 60° | : | 0.61 | 1.64 | 1.81 | 1.1 | 0.5 | 83° |
| ,, | ,, | ,, | ,, | ,, | ,, | 30° | : | 0.83 | 1.21 | 1.56 | 1.28 | 0.5 | 20° |
| ,, | ,, | ,, | ,, | ,, | 0.2 | 60° | : | 0.12 | 8.62 | 4.15 | 0.5 | 0.48 * | 25° |
| ,, | ,, | ,, | ,, | ,, | ,, | 30° | : | 0.07 | 14.0 | 5.29 | 0.5 | 0.38 * | 14° |

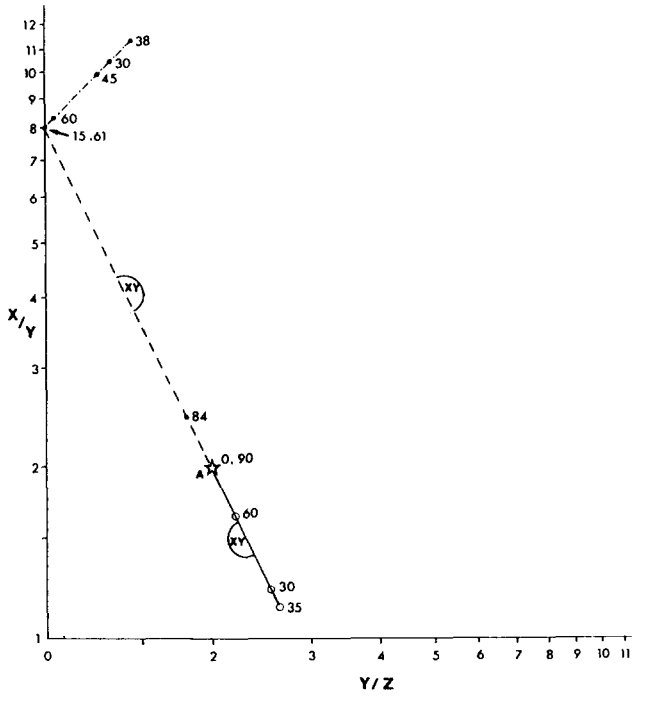


Fig. 13. Strain plots (see Fig. 11) for $XY$ principal-plane orientations ($Z_A$ parallel to layering), $Y_A = 1$ and $\xi'_{A1} = 0.5$. Reference strain (A) is starred; successive $\theta'_A$ values symbolled and numbered; solid line is $V = 5$ and broken line $V = 0.2$; arrow indicates axial interchange; dot–dash line indicates strain ellipses in the changed mode.

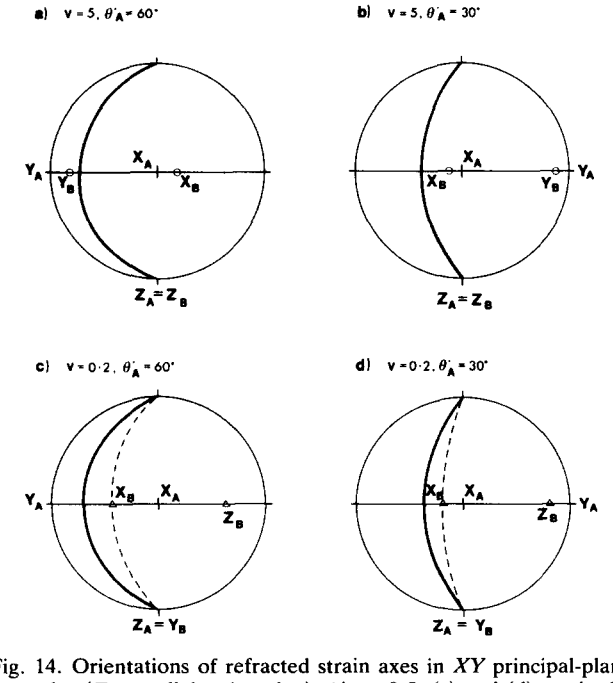


Fig. 14. Orientations of refracted strain axes in $XY$ principal-plane examples ($Z_A$ parallel to layering), $\xi'_{A1} = 0.5$; (c) and (d) are in the changed mode ($Y_B$ parallel to $Z_A$). Lower hemisphere equal area nets.

change of principal strain axes from layer A to B such that $Z_A = Y_B$ as asterisked in Table 4. Figure 14 shows the orientations of the principal strain axes in A and B for the examples of Table 4 indicated in Fig. 13; plots (c) and (d) are in the 'changed mode'.

### YZ *principal planes*

$X_A = X_B$ is parallel to $z$ of the layering. The method follows that described above for the $XY$ plane. In this case, $\xi'_{A2} = 1/Y_A^2 \cdot X_A$ and $\xi'_{A3} = 1/Z_A^2 \cdot X_A$, and similarly for B. Examples will again be given where $\xi'_{A2} = 0.5$ and $\xi'_{A3} = 2.0$ and $Y_A = 1$, with reference to Fig. 5. The results are given in Table 5, and plotted on the strain plot (Fig. 15).

The results are generally reciprocal to those described for the $XY$ planes. The $V = 5$ solid line demonstrates that the refracted strain ellipsoids become progressively prolate from $\theta'_A = 0$–35°, and then reverse in trend. The $V = 0.2$ broken lines give oblate ellipsoids, with axial change at $\theta'_A = 15$ and 61°. In the range $\theta'_A = 15$–61°, $Y_B = X_A$ as asterisked in Table 5. Figure 16 shows the orientations of principal axes for the examples of Table 5 and indicated in Fig. 15; plots (c) and (d) show axial interchange.

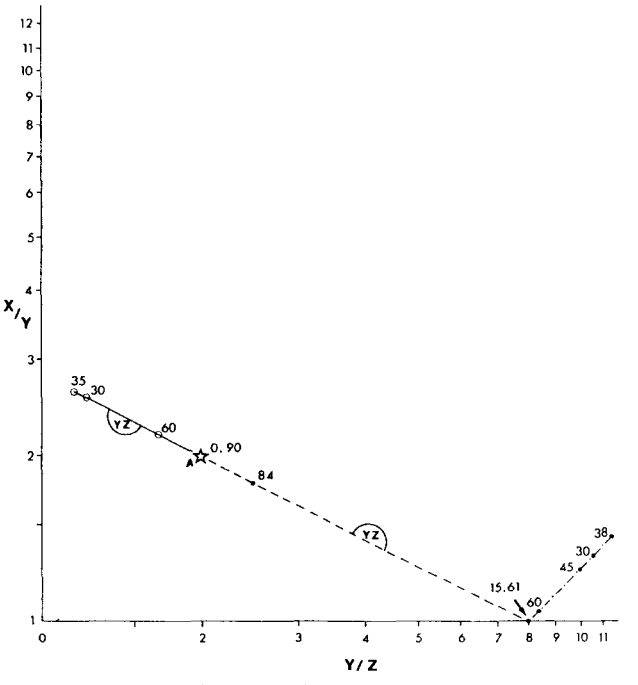


Fig. 15. Strain plots (see Fig. 11) for $YZ$ principal-plane orientations ($X_A$ parallel to layering), $Y_A = 1$ and $\xi'_{A2} = 0.5$. Reference strain (A) is starred; successive $\theta'_A$ values symbolled and numbered; solid line is $V = 5$ and broken line $V = 0.2$; arrow indicates axial interchange; dot–dash line indicates strain ellipses in the changed mode.

Table 5. Numerical results for $YZ$-plane solutions, $X$ parallel to layering

| $X_A$ | $Y_A$ | $Z_A$ | $\xi'_{A2}$ | $\xi'_{A3}$ | $V$ | $\theta'_A$ | : | $\xi'_{B2}$ | $\xi'_{B3}$ | $X_B$ | $Y_B$ | $Z_B$ | $\theta'_B$ |
|---|---|---|---|---|---|---|---|---|---|---|---|---|---|
| 2.0 | 1.0 | 0.5 | 0.5 | 2.0 | 5.0 | 60° | : | 0.61 | 1.64 | 2.0 | 0.91 | 0.55 | 83° |
| ,, | ,, | ,, | ,, | ,, | ,, | 30° | : | 0.83 | 1.21 | 2.0 | 0.78 | 0.64 | 20° |
| ,, | ,, | ,, | ,, | ,, | 0.2 | 60° | : | 0.12 | 8.62 | 2.08 | 2.0 | 0.24 * | 25° |
| ,, | ,, | ,, | ,, | ,, | ,, | 30° | : | 0.07 | 14.0 | 2.65 | 2.0 | 0.19 * | 14° |

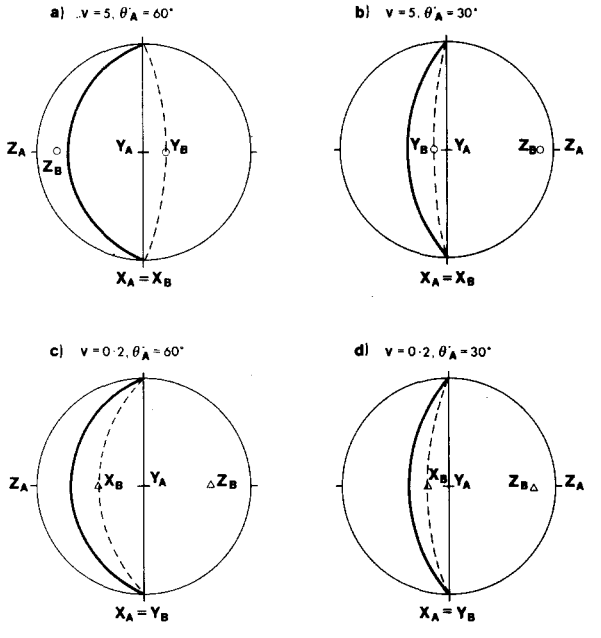


Fig. 16. Orientations of refracted strain axes in $YZ$ principal-plane examples ($X_A$ parallel to layering), $\xi'_{A2} = 0.5$; (c) and (d) are in the changed mode ($Y_B$ parallel to $X_A$). Lower hemisphere equal-area nets.

## GENERAL FINITE STRAIN REFRACTION

The present two-dimensional analysis can only be applied to planes which remain coplanar across viscosity contrasts during strain. All the examples have been restricted to cases where one principal strain axis is parallel to the layering interface. Because this axis is the same for all layers by definition, it follows that the principal plane perpendicular to the axis is consistent across viscosity contrasts.

Four separate cases have been considered: (1) $Y$ parallel to layering, $Y = 1$; (2) $Y$ parallel to layering, $Y \neq 1$; (3) $Z$ parallel to layering ($Y_A = 1 \neq Y_B$) and (4) $X$ parallel to layering ($Y_A = 1 \neq Y_B$). Examples could have been given for (3) and (4) where $Y_A \neq 1$.

A general oblique orientation of layering with respect to $X$, $Y$ and $Z$ in layer A cannot be considered by this theoretical model because there is no unique plane which has remained continuous and coplanar throughout strain across viscosity contrasts. Finite strain refraction in the general case will require three-dimensional solutions like the infinitesimal theory (Treagus 1981). In losing the advantage of the two dimensional illustration and the simplicity of the present Mohr-diagram solution, the results, when found, will prove more difficult to illustrate. Three-dimensional finite strain refraction theory is a subject for future research.

## GEOLOGICAL DISCUSSION

An application of the theoretical results to geological strain and cleavage patterns is conditional on the following criteria.

(1) Rocks are considered to approximate to Newtonian behaviour with an apparent constant (isotropic) viscosity.

(2) There is no volume loss. (However, the theory is readily adaptable to strain with dilation, if the dilation factor is constant for A and B).

(3) Bedding-plane interfaces retain adherence such that continuity exists.

(4) Layering is two-dimensionally oblique. One principal strain axis is parallel throughout the system, and lies in the interface plane.

Of these criteria (1) and (2) are considered as a reasonable starting point for a theoretical model. However, the assumption of isotropy may restrict the validity of the theory for large strains. With progressive finite strain and the associated development of a planar or linear fabric, an initially-homogeneous rock will become progressively anisotropic. This progressive anisotropy would be expected to influence incremental strain refraction during progressive strain (Cobbold 1976). An inclusion of a progressive anisotropy factor variably oblique to layering is beyond the scope of the present theory, but a possible direction for future research. Assuming an isotropic viscosity, estimates of rock viscosity are discussed below. Criterion (4) is not considered applicable to all deformed rocks by this author (see e.g. Treagus & Treagus 1981, Treagus 1981). Nevertheless much geological evidence does merit it as a useful (if only approximate) model; this evidence is given below.

In the proceeding discussion particular features of strain refraction are described with geological implications, concluding with a discussion of cleavage refraction.

### *Rock 'viscosity' ratios*

Shimamoto & Hara (1976) attempted to determine viscosity ratios in Japanese metamorphic rocks from wavelength–thickness ratios of folded quartz veins in different matrix rocks. Their data give the following

approximate mean $V$ values: 25 for quartz/mafic schist, 33 for quartz/psammitic schist and 125 for quartz/pelitic schist. Thus, a competence sequence can be demonstrated with respect to pelitic schist from quartz veins ($V = 125$), through mafic schist ($V = 5$) to psammitic schist ($V = 4$). There is no data on competent rocks such as quartzites and psammites but these are presumed to fall in the range $V = 5$–125 with respect to pelite. Thus, the theoretical ratios of $V = 5$ and 0.2 with respect to the reference viscosity which give maximum competence ratios of 25 would seem reasonable for sedimentary/metamorphic rocks of sandstone/shale or psammite/pelite range, although there is very little data to use as evidence for this claim.

*Evidence for two-dimensionally oblique strain*

Three symmetry types of finite strain ellipsoids and layering are possible in deformed rocks: (1) orthogonal or orthorhombic, (e.g. layer-parallel shortening); (2) two-dimensionally oblique or monoclinic, and (3) three-dimensionally oblique or triclinic. It is suggested that (1) is unlikely to operate throughout a deformation. While layer-parallel strains such as compactional flattening or layer-parallel compression prior to folding may exist in subhorizontal sediments, once the layers become folded they would proceed in two-dimensionally oblique strain, except perhaps, in certain positions such as fold hinge zones. Thus, the finite strain would be at least two-dimensionally oblique. The geological evidence for three-dimensionally oblique systems was given by Treagus & Treagus (1981) and Treagus (1981) as folds cross-cut, both axially and in profile, by their synchronous cleavage. However, in many areas of deformed layered rocks, the structural observations would appear to support a two-dimensionally oblique strain model, either completely or as a good approximation.

The most convincing geological evidence for two-dimensionally oblique strain is considered to be where sequences of folded layers have refracting and fanning cleavage intersecting layering parallel to fold or boudin axes. This is a common observation in many primary folds, so classical that it is sometimes assumed to be the general rule. Where the cleavage-bedding intersections are demonstrably parallel to the fold axes in contrasting lithologies, and cleavage refracts viewed in the fold-profile plane, the following conclusions would seem logical.

(1) Cleavages are approximately parallel to $XY$ planes.

(2) Fold axes are (a) parallel to a constant $Y$ axis, or (b) parallel to a constant $X$ axis, or (c) parallel to neither $X$ nor $Y$ but perpendicular to a constant $Z$ axis in the layering envelope plane.

Statement (1) bypassed any mechanical arguments on the relationship of strain and fabrics, but the conclusion seems valid on purely circumstantial grounds. In statement (2), the situation (a) might be expected most commonly. Evidence for (b) should be given by extensional structures parallel to fold axes, and for (c) by lineations in the cleavage planes oblique to fold axes, variably in different lithologies.

The geological evidence for two-dimensionally oblique strain should be collated for all lithologies. The presence or absence of a strong linear structure in one layer alone may not indicate the total or 'bulk' strain axes for reasons given in the next sections.

*Strain variation and refraction*

The underlying control of strain refraction, in theory, is the criterion that the shear strain ratio at an interface is equal to the inverse viscosity ratio (see also Cobbold, this issue). A relative increase in viscosity implies an equivalent decrease in shear strain, and vice versa. From this factor alone, it follows that strain cannot be homogeneous across viscosity contrasts if there is shear strain parallel to layering. The change of strain is accomplished by refraction of strain axes and changes in principal strain values. These principles apply to strain refraction in any layered system where the principal finite strain axes are not orthogonal with respect to layer interfaces.

From the preceding theoretical results for strain refraction in two-dimensionally oblique systems, three interrelated features can be identified.

(1) Two principal finite strain axes will refract, layer to layer within one principal plane: therefore two principal planes will refract.

(2) In the two-dimensional view ($XY$, $XY$ or $YZ$ principal planes), strain ellipses will change shape from layer to layer.

(3) In three dimensions, strain ellipsoids will change their shape factors ($k$) from layer to layer. The only exception is the case where *all* refracting ellipsoids have $k = 1$, only true for $XZ$ plane views and $Y = 1$ parallel to interface.

The above features were illustrated theoretically in comparison to a reference layer A (chosen strain values given by Tables 2–5). The results are thus specific to the choice of the reference strain value, orientation and viscosity ratios. Any geological application will be dependent on the justification of the reference strain.

The concept of the reference layer may be applied to rocks in two ways. (i) The reference layer may be any layer in a multilayered sequence, having a known strain state (value and orientation). Strain states may then be derived in adjacent layers of estimated viscosity (competence) ratio—see previous discussion of rock viscosity. (ii) The reference layer may be viewed, conceptually, as a layer of average (bulk) characteristics, having a mean competence and representing the bulk or regional finite strain. This approach may be useful for an 'over-view' of strain refraction in varied lithologies, to derive some qualitative trends of strain ellipsoid orientation, size and shape in particular rock types. The geological implications following this approach are investigated now.

Consider a simple profile view of contrasting lithologies (verified as two-dimensionally oblique).

Within a sequence with maximum competence contrast of 25, a range of strain ellipse shapes might be expected as illustrated in Fig. 6. The competent layers should show little strain, the incompetent layers intense strain dominated by layer-parallel shear. The range of strain orientation within a competence range of 100 might be as indicated by the refraction of $X$ in Fig. 10. It might be expected that strain data from contrasting lithologies would indicate such dramatic differences in finite strain, controlled largely by lithology. The author knows of no such results. The implications of the change in strain value and orientation to cleavage refraction in rocks is discussed in the next section.

A single two-dimensional view of strain refraction in contrasting lithologies will not reveal the total strain refraction pattern: for this, knowledge of the third dimension is necessary. In general, it might be expected that strong variations of strain ellipsoid shapes, indicated by differences in $k$ factors, would occur in different lithologies. Certain lithologies might exhibit prolate-field strain and others oblate-field strain.

A critical point of strain refraction was illustrated at the coordinates of Figs. 11, 13 and 15 where $k = 0$ or $\infty$ ($X = Y$ or $Y = Z$) for particular layers. These are the points of *axial interchange* beyond which strain axes in the 'changed mode' occur: the third-dimension strain axis ($Y \neq 1$ or $X$ or $Z$) becomes a different principal axis in the refracted ellipsoid. Axial interchange represents an extreme form of strain ellipsoid refraction which would only be apparent from three-dimensional observation. In rocks it might be predicted for particular orientations of particular lithologies, as an anomaly. For example compare the two cases $Y_A > 1$ or $X_A$ parallel to the third dimension in the layering plane (Figs. 12b and 16c), each a possible fold axis. For the former, the anomaly (axial interchange) would occur in certain competent layers where the local $X$ direction would be parallel to the regional $Y$ = fold axis. For the latter the anomaly would be in certain competent layers where the local $X$ direction was perpendicular to the regional $X$ = fold axis. Thus in rocks, the knowledge that there was some extension parallel to fold axes together with strain data from a single lithology might lead to incorrect assumptions of the regional principal strain directions.

A final feature of strain refraction is that the strain in particular layers is rotational. Figure 10 illustrates the rotation of principal strain axes in particular layers by a comparison of infinitesimal and finite strain trajectories. In the least competent layers, the strain history may be approximated to the special form of rotational strain (simple shear) by neglecting the layer-orthogonal strain components. Layers $V = 0.2$ and 0.1 in Fig. 10(b) would approximate to simple shear of $\gamma = 6.2$ and 12, respectively. Such approximations may prove valid as a means of understanding the nature of strain in markedly incompetent layers.

*Cleavage refraction and fabric changes*

There is a paucity of strain data published for contrasting layers with cleavage refraction. Most geological strain data come from statistical studies in a particular lithology (assumed homogeneous) where strain markers abound. If perfect strain markers were present in all lithologies with refracting cleavages, much of the controversy on the relationship of cleavage and strain might be resolved and the present theory tested. In the meantime, there remains considerable dispute about the relationship of strain to cleavages of varied morphology, as summarized in the Introduction. While a simple application of the present strain-refraction results to cleavage refraction patterns in contrasting lithologies may be considered unjustified by many geologists, it might be a useful empirical test of the validity of qualitative comparisons of macroscopic cleavage and strain. Such tests have been applied to strain and cleavage associated with folds (Dieterich 1969), but not recently to cleavage refraction independent of folding.

The preceding strain refraction patterns will now be used to infer cleavage patterns on the assumptions that cleavages are subparallel to local $XY$ planes (except where $k \gg 1$), the strength of cleavage is controlled by the degree of strain, and stretching/mineral lineations are subparallel to $X$ axes. Thus the $XZ$ strain ellipses in Fig. 6 may be considered indicative of the orientation and strength of cleavage in lithologies with relative competence 5 and 0.2 (a competent/incompetent ratio of 25). Poor cleavage might be inferred for competent layers and intense cleavage for incompetent layers. The effect of competence on cleavage orientation is represented in Fig. 10 which simulates a maximum competent/incompetent ratio of 100. The pattern of refraction of trace 3 (Fig. 10a) from subnormal to layering towards progressively acute cleavage-bedding angles, strongly resembles cleavage refraction in upward-graded rocks (e.g. Fig. 17a). Associated with angular cleavage refraction simulated by Fig. 10 would be a progressive increase in cleavage intensity as competence decreases.

The predicted relationships of cleavage intensity and orientation to lithology may be summarized as two generalized trends from the mean (bulk) state.

*Trend 1.* With increasing relative competence the cleavage should refract to bedding-perpendicular or bedding-parallel; (bedding-perpendicular for shortened layers, bedding-parallel for elongated layers). In layers of exceptionally high relative competence, cleavage should be absent.

*Trend 2.* With decreasing relative competence, the cleavage should refract towards the bedding plane, and increase in intensity. In layers of exceptional incompetence, cleavage may be an intense foliation subparallel to bedding.

These two trends predicted from the theoretical results would seem to be verified by observation in single-deformed contrasting lithologies (e.g. Fig. 17). Trend 1 is the generalized trend for psammitic rocks and trend 2 for pelitic rocks (Fig. 17b), but equally it is observed that the morphology of trend 1 is spaced (e.g. 'fracture' cleavage) whereas trend 2 is penetrative (slaty). Are these morphological differences a result of

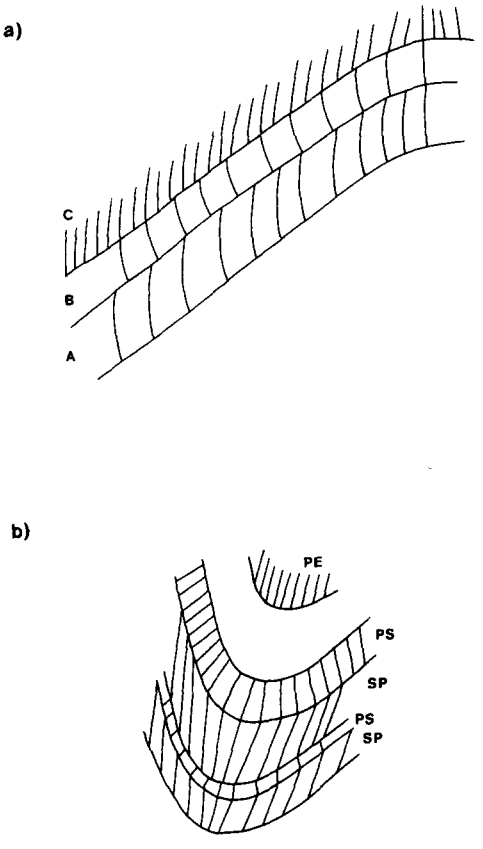


Fig. 17. Schematic cleavage refraction patterns in natural folds. (a) Cleavage in two graded layers (A & B) and mudstone (C) after Treagus (1982, fig. 5). (b) Cleavage in folded psammite (PS) semipelite (SP) and pelite (PE) after Treagus (1982, fig. 6).

mineralogical differences in contrasting layers, such as the presence or absence of phyllosilicates vs quartz? Or could it be argued that it is the degree of strain achieved in a particular lithology (more in phyllosilicate-rich pelites than in psammites) which controls the type of cleavage morphology? Studies of the evolution of slaty cleavage (Roy 1978, Piqué 1982) from an uncleaved to cleaved state demonstrate the progressive decrease of cleavage-domain spacing towards a penetrative fabric, within a single lithology. Thus, cleavages of various morphologies might be regarded as occupying a cleavage deformation path from spaced to penetrative (continuous) cleavage, along which particular lithologies have progressed to different points according to their finite strain states.

Such are the predicted two-dimensional features of cleavage refraction in rocks. In three dimensions, changes in strain ellipsoid shape from layer to layer may give rise to a range of related cleavage and lineation fabrics. It might be assumed that the refraction patterns seen in two dimensions (e.g. in a fold profile plane) might be projected simply into three dimensions. In such a model, cleavages would refract about a constant axis, the fold axis ($Y$), with extension lineations ($X$) perpendicular to the cleavage-bedding intersection ($Y$). However, this model of cleavage refraction is only perfectly verified, theoretically, when $Y = 1$ and all refracting strain ellipsoids are plane strain, $k = 1$. For the more general strain relationships of $Y \neq 1$ or $X$ or $Z$ parallel to layering, strong variations in ellipsoid $k$ values and local axial interchange are expected to affect the nature of cleavage and its attitude. Cleavages with stretching lineations would be expected in rocks where $k \approx 1$, cleavage without clear lineation where $k \ll 1$, and lineations without cleavage as $k \gg 1$. Cleavage and lineation refraction might be anomalous in localities of axial interchange.

Some generalized predictions are given on the relationship of cleavages and lineations for four two-dimensionally oblique strain configurations.

(1) $Y$ = *fold axis, bulk* $Y > 1$ (Figs. 11 and 12). Bulk cleavage-bedding intersections are parallel to fold axes, extension lineations (if present) perpendicular. Competent layers show weak refracted cleavage (trend 1), cleavage-bedding intersections parallel to fold axes (generally local $Y$) and lineations ($X$) perpendicular to fold axes or anomalously parallel to fold axes. Incompetent layers have a strong refracted cleavage according to trend 2 and stretching lineations perpendicular to cleavage-bedding intersections and fold axes.

(2) $Y$ = *fold axis, bulk* $Y < 1$ (Figs. 11 and 12). Bulk cleavage-bedding intersections are parallel to fold axes, extension lineations perpendicular. Bulk fabric planar to linear according to $Y$ value. Competent layers show weak refracted cleavage (trend 1) with extension lineation perpendicular to fold axes or anomalous cross cleavage (not fully assessed with respect to the cross folding in $Y$). Incompetent layers show a strong refracted cleavage (trend 2) with strong stretching lineations perpendicular to cleavage-bedding intersections and fold axes.

(3) $X$ = *fold axis, bulk* $Y = 1$ *oblique to bedding* (Figs. 15 and 16). Bulk cleavage bedding intersections, parallel to fold axes, are parallel to extension lineations. Competent layers have a weak linear fabric parallel to fold axes. Incompetent layers have a strongly-planar refracted cleavage probably lacking an extension lineation; if present, lineations will be parallel to fold axes or anomalously perpendicular.

(4) $Z$ *parallel to layering, bulk* $Y = 1$ *oblique* (Figs. 13 and 14). Bulk cleavage- bedding intersections are parallel to fold axes oblique to stretching lineations. Competent layers have a weak planar fabric with lineations (if present) perpendicular to cleavage-bedding intersections. Incompetent layers have strong linear fabrics at acute angles to fold axes, lying in the plane of bulk cleavage. Anomalies of axial interchange may give local 'secondary' fabrics. These predictions are only applicable to uniformly-bedded rocks or hinge zones of folds; the limbs would be three-dimensionally oblique.

The summaries of characteristic relationships between planar and linear fabrics in contrasting lithologies in particular bulk strain states may be useful in determining the orientation and relative values of bulk strain in deformed rocks. Despite the strong variations from planar to linear fabrics predicted, and the occurrence of certain anomalous fabrics, the two fabric trends with increasing and decreasing competence would appear to

dominate fabric refraction. The fabric, whether planar, linear or anomalous, will be weak in relatively competent layers and strong in relatively incompetent layers.

*Cleavage refraction related to folds*

The features of cleavage and lineation refraction have been predicted for specific two-dimensionally oblique strain configurations with respect to fold axis orientation. However folding is not a necessity for strain and cleavage refraction. The refraction arises from compatibility theory in obliquely strained layers which might be uniformly dipping or parts of folds (e.g. limbs). Thus, the strain or cleavage refraction of curve 3 of Fig. 10(a) entirely results from the chosen strain state (shaded layer) and viscosity ratios; it is equally applicable to a regularly dipping sequence of rocks or part of a fold limb such as in Fig. 17(a). The fabric relationships are described in relation to fold axes simply because contrasting lithologies are commonly folded and fold axes are the major structural data with which to compare the fabrics. Apart from localized strain and cleavage in fold hinge zones, the process of folding is here viewed as a periodic and variable body rotation which imposes variable systems of oblique strain. It is the obliquity of strain within layers of variable competence which is proposed as the mechanism for strain and cleavage refraction in the limbs of folds, not the mechanism of folding.

This approach clearly differs from the methods of fold analysis based on particular strain models in folding (Ramsay 1967, Hobbs 1971, Hudleston 1973); such models do not consider whether particular strain patterns are compatible for contrasting layers. However, some fold models are rooted in empirical observations from experimental models and rocks, and may be good approximations of strain behaviour for particular relative competencies. The patterns of strain described in this paper for relatively high competencies approximate well to tangential longitudinal strain, and for relatively low competencies to flexural flow (simple shear); these are Ramsay's (1967) two principal models of strain in folded layers. In contrast the model of folding followed by homogeneous strain ('flattening' of Ramsay 1962, 1967) or folding with simultaneous 'flattening' (Hudleston 1973) are not consistent with the present strain refraction results if competence contrasts exist within the folding sequence; 'flattening' should be inhomogeneous. The extent to which fold geometry and cleavage refraction data may be combined (following Treagus 1982) to provide estimates of local strain and competence ratios in natural folds, is the subject of current research.

*Fabrics in polyphase deformation*

The foregoing discussion of cleavage and lineation refraction in folded or unfolded rocks relates specifically to primary deformation. The investigation of the relationship of cleavage and strain in the Introduction was restricted to primary/first cleavage. For secondary crenulation cleavage or schistosity, the relationships of schistosities and lineations would not be independent of the earlier strain and fabric. Thus the predicted relationships for cleavage refraction would appear inapplicable to rocks which suffered polyphase deformation. However, some of the general features may prove relevant to understanding the progressive development of strain and fabric in multiply deformed rocks. The intensity of a fabric was suggested to be a function of relative competence, and this factor would operate throughout a complex deformation history if competence contrasts remained constant. Thus, a competent psammitic layer might be expected to develop weak fabrics for each deformation phase (or a single cumulative fabric of increasing intensity with each phase). In contrast, an incompetent pelitic layer with a strong first cleavage would subsequently deform in relatively intense strain, so might be expected to develop a strong secondary fabric. The total strain in such contrasting lithologies is thus expected to follow the two competence trends. However, it is probable that competence ratios do not remain fixed during polyphase deformation with metamorphism. As competence ratios approach unity incremental strain would approach the state of homogeneous strain.

## CONCLUSIONS

The following conclusions are drawn for strain variation in contrasting Newtonian viscous layers.

(1) In all contrasting multilayers, except those where one principal strain axis is perpendicular to interface planes, strain will be inhomogeneous.

(2) In general, finite strain will vary in inverse proportion to viscosity or competence.

(3) The principal strain axes will refract from layer to layer, and thus the principal planes (e.g. $XY$) will refract. In this theory the refraction can be considered as two-dimensional about an axis in layering which is a principal strain.

(4) In all cases except plane strain with $Y = 1$ parallel to layering, there will be a change of ellipsoid shape defined by the $k$ value. Oblate ellipsoids may refract to prolate ellipsoids at competence interfaces.

(5) In some cases, extremes of shape change arise where the ellipsoid has passed through a $k = 0$ or $k = \infty$ threshold, and principal axes have interchanged with respect to adjacent layers.

(6) Compatible states of finite strain will generally have developed by rotational incremental strain.

(7) The features of strain refraction described are similar to the features of cleavage in rocks with competence contrast: weak cleavage (spaced) at high angle to bedding in competent rocks; strong cleavage (slaty) at more acute angles to bedding in incompetent rocks.

If cleavages are assumed to be subparallel to $XY$ planes of finite strain and extension lineations are parallel to $X$, further geological conclusions may be drawn.

(8) Cleavage perpendicular or parallel to bedding will not refract through contrasting lithologies. (This

was observed by Sorby (1853), quoted in the Introduction.)

(9) Cleavage oblique to bedding in one lithology must refract through contrasting lithologies.

(10) Uniformly-oriented cleavage should only occur within a homogeneous rock of uniform dip.

(11) Fabrics may change from planar to linear at lithological boundaries.

(12) The orientation of a cleavage and/or extension lineation in a single lithology may not indicate the bulk or regional strain axes.

*Acknowledgements*—This paper is the result of research undertaken during a Natural Environmental Research Council Research Fellowship held at Manchester, 1979–1981. I should like to acknowledge the facilities provided by the Geology Department at Manchester and the Honorary status which enabled me to write the paper. I have benefited from the criticism of Jack Treagus, Brian Bayly and Peter Cobbold.

## REFERENCES

Borradaile, G. J., Bayly, M. B. & Powell, C. McA. (editors) 1982. *Atlas of Deformation and Metamorphic Rock Fabrics*. Springer, New York.

Cobbold, P. R. 1976. Mechanical effects of anisotropy during large finite deformations. *Bull. Soc. geol. Fr.* **18**, 1497–1510.

Cobbold, P. R. 1983. Kinematic and mechanical discontinuity at a coherent interface. *J. Struct. Geol.* **5**, 341–349.

Dennis, J. G. 1967. *International Tectonic Dictionary*. Mem. Am. Ass. Petrol. Geol. **7**.

Dieterich, J. H. 1969. Origin of cleavage in folded rocks. *Am. J. Sci.* **267**, 155–165.

Dieterich, J. H. & Carter, N. L. 1969. Stress history of folding. *Am. J. Sci.* **267**, 129–154.

Flinn, D. 1962. On folding during three-dimensional progressive deformation. *Q. Jl geol. Soc. Lond.* **118**, 385–433.

Geiser, P. A. 1974. Cleavage in some sedimentary rocks of the central Valley and Ridge province, Maryland. *Bull geol. Soc. Am.* **85**, 1399–1412.

Ghosh, S. K. 1982. The problem of shearing along axial plane foliations. *J. Struct. Geol.* **4**, 63–67.

Goguel, J. 1982. Une interprétation méchanique de la réfraction de la schistosité. *Tectonophysics*, **82**, 125–143.

Gray, D. R. 1981. Compound tectonic fabrics in singly-folded rocks from Southwest Virginia, U.S.A. *Tectonophysics*, **78**, 229–248.

Groshong, R. H. Jr. 1976. Strain and pressure solution in Martinsburg slate, Delaware Water Gap, New Jersey. *Am J. Sci.* **276**, 1131–1146.

Harker, A. 1896. On slaty cleavage and allied rock structures with special reference to the mechanical theories of their origin. *Rep. Br. Ass. Adv. Sci.* (1885), 813–852.

Hobbs, B. E. 1971. The analysis of strain in folded layers. *Tectonophysics* **11**, 329–375.

Hobbs, B. E., Means, W. D. & Williams, P. F. 1982. The relationship between foliation and strain: an experimental investigation. *J. Struct. Geol.* **4**, 411–428.

Hudleston, P. J. 1973. Fold morphology and some geometrical implications of theories of fold development. *Tectonophysics* **16**, 1–46.

Leith, C. K. 1905. Rock cleavage. *Bull. U.S. geol. Surv.* **239**, 1–216.

Leith, C. K. 1914. *Structural Geology*. Constable & Co., London.

Maxwell, J. C. 1962. Origin of slaty and fracture cleavage in the Delaware Water Gap area, New Jersey and Pennsylvania. *Mem. geol. Soc. Am., Buddington volume*, 281–311.

Means, W. D. 1975. Natural and experimental microstructures in deformed micaceous sandstones. *Bull. geol. Soc. Am.* **86**, 1211–1229.

Means, W. D. 1977. Experimental contributions to the study of foliations in rocks: a review of research since 1860. *Tectonophysics* **39**, 329–354.

Mukhopadhyay, D. 1965. Development of schistosity in flexural folds. *Geol. Mag.* **102**, 415–417.

Piqué, A. 1982. Relations between stages of diagenetic and metamorphic evolution and the development of a primary cleavage in the north western Moroccan Meseta. *J. Struct. Geol.* **4**, 491–500.

Powell, C. McA. 1972. Tectonic dewatering and strain in the Michigamme slate, Michigan. *Bull. geol. Soc. Am.* **83**, 2149–2158.

Powell, C. McA. 1979. A morphological classification of rock cleavage. *Tectonophysics* **58**, 21–34.

Ramberg, H. 1962. Contact strain and folding instability of a multilayered body under compression. *Geol. Rdsch.* **51**, 405–439.

Ramsay, J. G. 1962. Mechanics of formation of 'similar' type folds. *J. Geol.* **70**, 309–327.

Ramsay, J. G. 1967. *Folding and Fracturing of Rocks*. McGraw-Hill, New York.

Roberts, D. 1971. Abnormal cleavage patterns in fold hinge zones from Varanger peninsula, Northern Norway. *Am. J. Sci.* **271**, 170–180.

Roberts, D. & Strömgård, K. E. 1972. A comparison of natural and experimental strain patterns around fold hinge zones. *Tectonophysics* **14**, 105–120.

Roy, A. B. 1978. Evolution of slaty cleavage in relation to diagenesis and metamorphism: a study from the Hunruckschiefer. *Bull. geol. Soc. Am.* **89**, 1775–1785.

Sharpe, D. 1849. On slaty cleavage. *Q. Jl geol. Soc. Lond.* **5**, 111–115.

Shimamoto, T. & Hara, I. 1976. Geometry and strain distribution of single-layer folds. *Tectonophysics* **30**, 1–34.

Siddans, A. W. B. 1972. Slaty cleavage—a review of research since 1815. *Earth Sci. Rev.* **8**, 205–232.

Sorby, H. C. 1853. On the origin of slaty cleavage. *Edinb. New Philos. J.* **55**, 137–148.

Treagus, J. E. & Treagus, S. H. 1981. Folds and the strain ellipsoid: a general model. *J. Struct. Geol.* **3**, 1–17.

Treagus, S. H. 1973. Buckling stability of a viscous single-layer system, oblique to the principal compression. *Tectonophysics* **19**, 271–289.

Treagus, S. H. 1981. A theory of stress and strain variations in viscous layers, and its geological implications. *Tectonophysics* **72**, 75–103.

Treagus, S. H. 1982. A new isogon-cleavage classification and its application to natural and model fold studies. *Geol. J.* **17**, 49–64.

Tullis, T. E. 1976. Experiments on the origin of slaty cleavage and schistosity. *Bull. geol. Soc. Am.* **87**, 745–753.

Tullis, T. E. & Wood, D. S. 1975. Correlation of finite strain from both reduction bodies and preferred orientation of mica in slate from Wales. *Bull. geol. Soc. Am.* **86**, 632–638.

White, S. H. & Knipe, R. J. 1978. Microstructure and cleavage development in selected slates. *Contr. Miner. Petrol.* **66**, 165–174.

Williams, P. F. 1976. Relationships between axial-plane foliations and strain. *Tectonophysics* **30**, 181–196.

Williams, P. F. 1977. Foliation: a review and discussion. *Tectonophysics* **39**, 305–328.

Wilson, G. 1961. The tectonic significance of small scale structures. *Ann. Soc. Geol. Belg. Bull.* **84**, 423–548.

Wood, D. S. 1974. Current views on the development of slaty cleavage. *A. Rev. Earth Planet Sci.* **2**, 1–37.

Wood, D. S. & Oertel, G. 1980. Deformation in the Cambrian slate belt of Wales. *J. Geol.* **88**, 285–308.

## APPENDIX 1

Criterion (6), given in "Theoretical model of two-dimensional finite strain refraction" is that $\tau_{Ax} = \tau_{Bx}$ at the interface A to B. Consequently $\eta_A\dot{\gamma}_{Ax} = \eta_B\dot{\gamma}_{Bx}$ can be written, where $\eta$ is Newtonian viscosity and $\dot{\gamma}$ shear strain rate; this simplifies to $\dot{\gamma}_{Ax}/\dot{\gamma}_{Bx} = V$ where $V = \eta_B/\eta_A$. The integral of this ratio with time is $\gamma_{Ax}/\gamma_{Bx} = V$ if $V$ remains constant in time. This integration is tested as follows.

Consider an instant after the first small increment of deformation such that in A and B the shear strains $\gamma^{i}_{Ax}/\gamma^{i}_{Bx} = V$ (Treagus 1981). Add a small increment of shear strain (simple shear) in the ratio $d\gamma_{Ax}/d\gamma_{Bx} = V$ so that the new shear strain $\gamma^{ii}$ may be written $\gamma^{ii} = \gamma^{i} + d\gamma$; it is apparent that $\gamma^{ii}_{Ax}/\gamma^{ii}_{Bx} = V$. Now consider a small increment of normal strain (pure shear) in $x$ and $y$. The change in angles of shear may be expressed (Ramsay 1967, p. 67) in the form $\tan\theta' = \tan\theta\ (\lambda_2/\lambda_1)^{1/2}$. The above shear strains being tangents would be distorted to 'new' shear strains $\gamma^{iii}$

$$\gamma^{iii}_{Ax} = \gamma^{ii}_{Ax}\,(\zeta_{Ax}/\zeta_{Ay})^{1/2} \text{ and } \gamma^{iii}_{Bx} = \gamma^{ii}_{Bx}\,(\zeta_{Bx}/\zeta_{By})^{1/2}.$$

$\zeta_{Ax}$, $\zeta_{Ay}$ and $\zeta_{Bx}$, $\zeta_{By}$ are principal quadratic elongation increments in the small increment of pure shear in A and B. For continuity $\zeta_{Ax} = \zeta_{Bx}$ and $\zeta_{Ay} = \zeta_{By}$. Thus, $\gamma^{iii}_{Ax}/\gamma^{iii}_{Bx} = \gamma^{ii}_{Ax}/\gamma^{ii}_{Bx} = V$. Therefore, during the progressive development of shear strain, the ratio of shear strains at

the interface remains equal to $V$ despite the effect of normal strain components. For a fuller treatment of interface problems, in both Newtonian and non-Newtonian materials, see Cobbold (this issue).

## APPENDIX 2

The relationships given by the laws of continuity (5) and (6) in the section "Theoretical model of two-dimensional finite strain refraction" can be written in terms of principal quadratic elongations and angles, defined in Fig. 2. Adopting reciprocal quadratic elongations (Ramsay 1967 p. 66) as most convenient, the following equations can be written.

$$\lambda'_{Ax} = \frac{(\lambda'_{A3} + \lambda'_{A1}) - (\lambda'_{A3} - \lambda'_{A1})\cos 2\theta'_A}{2} \quad (1)$$

$$\gamma'_{Ax} = \frac{(\lambda'_{A3} - \lambda'_{A1})\sin 2\theta'_A}{2} \quad (2)$$

where $\gamma'_{Ax} = \gamma_{Ax}.\lambda'_{Ax}$. Because of the condition of plane strain given by law 4, $\lambda'_{A3} = 1/\lambda'_{A1}$. Thus

$$\lambda'_{Ax} = \frac{(1 + \lambda'^2_{A1}) - (1 - \lambda'^2_{A1})\cos 2\theta'_A}{2\lambda'_{A1}} \quad (3)$$

and

$$\gamma'_{Ax} = \frac{(1 - \lambda'^2_{A1})\sin 2\theta'_A}{2\lambda'_{A1}}. \quad (4)$$

Similarly,

$$\lambda'_{Bx} = \frac{(1 + \lambda'^2_{B1}) - (1 - \lambda'^2_{B1})\cos 2\theta'_B}{2\lambda'_{B1}} \quad (5)$$

and

$$\gamma'_{Bx} = \frac{(1 - \lambda'^2_{B1})\sin 2\theta'_B}{2\lambda'_{B1}}. \quad (6)$$

From law 5, $\lambda'_{Ax} = \lambda'_{Bx}$; hence

$$\frac{(1 + \lambda'^2_{A1}) - (1 - \lambda'^2_{A1})\cos 2\theta'_A}{2\lambda'_{A1}} = \frac{(1 + \lambda'^2_{B1}) - (1 - \lambda'^2_{B1})\cos 2\theta'_B}{2\lambda'_{B1}} \quad (7)$$

From law 6 $\gamma'_{Ax}/\gamma'_{Bx} = V$; hence

$$\frac{(1 - \lambda'^2_{A1})\sin 2\theta'_A}{2\lambda'_{A1}} = \frac{V(1 - \lambda'^2_{B1})\sin 2\theta'_B}{2\lambda'_{B1}}. \quad (8)$$

From equations (7) and (8) it is clear that if the size and orientation of the strain ellipse is known in one layer, it can be derived in an adjacent layer of known viscosity ratio. It will be assumed that A is the known material: thus $\lambda'_{A1}$, $\theta'_A$ and $V$ are known variables and $\lambda'_{B1}$ and $\theta'_B$ are unknown. Explicit solutions $\lambda'_{B1} = f_1(\lambda'_{A1}, \theta'_A, V)$ and $\theta'_B = f_2(\lambda'_{A1}, \theta'_A, V)$ will not be derived because the algebra is lengthy and involved. Instead, solutions $\lambda'_{B1} = f_3(\lambda'_{Ax}, \gamma'_{Ax}, V)$ and $\theta'_B = f_4(\lambda'_{Ax}, \gamma'_{Ax}, V)$ will be obtained.

The known variables $\lambda'_{Ax}$ and $\gamma'_{Ax}$ will be termed $L$ and $S$, respectively, as given by (3) and (4). Thus, (7) and (8) can be written

$$\frac{(1 + \lambda'^2_{B1}) - (1 - \lambda'^2_{B1})\cos 2\theta'_B}{2\lambda'_{B1}} = L \quad (9)$$

$$\frac{(1 - \lambda'^2_{B1})\sin 2\theta'_B}{2\lambda'_{B1}} = S/V. \quad (10)$$

Squaring (10) gives

$$\sin^2 2\theta'_B = \frac{4S^2(\lambda'^2_{B1})}{V^2(1 - \lambda'^2_{B1})^2} \quad (11)$$

and by trigonometric substitution

$$\cos^2 2\theta'_B = \frac{V^2(1 - \lambda'^2_{B1})^2 - 4S^2\lambda'^2_{B1}}{V^2(1 - \lambda'^2_{B1})^2}. \quad (12)$$

Squaring (9)

$$\cos^2 2\theta'_B = \frac{(\lambda'^2_{B1} - 2L\lambda'_{B1} + 1)^2}{(1 - \lambda'^2_{B1})^2}. \quad (13)$$

Equating (12) and (13)

$$L\lambda'^2_{B1} - \lambda'_{B1}(1 + L^2 + S^2/V^2) + L = 0. \quad (14)$$

This may be written as a simple quadratic equation

$$\lambda'^2_{B1} - M\lambda'_{B1} + 1 = 0, \quad (15)$$

where

$$M = \frac{1 + L^2 + S^2/V^2}{L}. \quad (16)$$

Hence

$$\lambda'_{B1} = M - (M^2 - 4)^{1/2} \quad (17)$$

and

$$\lambda'_{B3} = M + (M^2 - 4)^{1/2}. \quad (18)$$

Substitution for $\lambda'_{B1}$ in (10) gives

$$\sin 2\theta'_B = \frac{2S}{V(M^2 - 4)^{1/2}}. \quad (19)$$

Similarly, from (9)

$$\cos 2\theta'_B = \frac{M - 2L}{(M^2 - 4)^{1/2}}. \quad (20)$$

From (19) and (20) $\theta'_B$ can be expressed directly in terms of $S$, $L$ and $V$:

$$\tan 2\theta'_B = \frac{2SLV}{V^2 - V^2L^2 + S^2}. \quad (21)$$

The above equations for $\lambda'_{B1}$, $\lambda'_{B3}$ and $\theta'_B$ are given in summary in Table 1.